Human Cytomegalovirus Major Immediate-Early 1 Protein Targets Host Chromosomes by Docking to the Acidic Pocket on the Nucleosome Surface

Running title: hCMV IE1 Protein Targets the Nucleosome Surface

Katrin Mücke,[a] Christina Paulus,[a] Katharina Bernhardt,[a]* Katrin Gerrer,[a]* Kathrin Schön,[a] Alina Fink,[a] Eva-Maria Sauer,[a]* Alexandra Asbach-Nitzsche,[a] Thomas Harwardt,[a] Bärbel Kieninger,[b] Werner Kremer,[b] Hans Robert Kalbitzer,[b] Michael Nevels[a]#

Institute for Medical Microbiology and Hygiene, University of Regensburg, Regensburg, Germany[a]; Institute of Biophysics and Physical Biochemistry, University of Regensburg, Regensburg, Germany[b]

#Address correspondence to Michael Nevels, michael.nevels@ukr.de.

*Present address: Katharina Bernhardt, Department of Microbiology and Immunobiology, Harvard Medical School, Boston, Massachusettes, USA; Katrin Gerrer, Faculty of Biology, University of Freiburg, Freiburg, Germany; Eva-Maria Sauer, Department of Neurology, Friedrich-Alexander University of Erlangen-Nürnberg, Erlangen, Germany.

K.M. and C.P. contributed equally to this work.

Word count: 250 (abstract), 9,524 (text excl. abstract, references, and legends)

Abstract

The 72-kDa immediate-early 1 (IE1) protein encoded by human cytomegalovirus (hCMV) is a nuclear-localized promiscuous regulator of viral and cellular transcription. IE1 has long been known to associate with host mitotic chromatin, yet the mechanisms underlying this interaction have not been specified. In this study, we identify the cellular chromosome receptor for IE1. We demonstrate that the viral protein targets human nucleosomes by directly binding to core histones in a nucleic acid-independent manner. IE1 exhibits two separable histone interacting regions with differential binding specificities for H2A-H2B and H3-H4. The H2A-H2B binding region was mapped to an evolutionary conserved ten-amino-acid motif within the chromatin tethering domain (CTD) of IE1. Results from experimental approaches combined with molecular modeling indicate that the IE1 CTD adopts a β-hairpin structure docking with the acidic pocket formed by H2A-H2B on the nucleosome surface. IE1 binds to the acidic pocket in a way similar to the latency-associated nuclear antigen (LANA) of the Kaposi's sarcoma-associated herpesvirus. Consequently, the IE1 and LANA CTDs compete for binding to nucleosome cores and chromatin. Our work elucidates in detail how a key viral regulator is anchored to human chromosomes and identifies the nucleosomal acidic pocket as a joint target of proteins from distantly related viruses. Based on the striking similarities between the IE1 and LANA CTDs and the fact that nucleosome targeting by IE1 is dispensable for productive replication even in "clinical" strains of hCMV, we speculate that the two viral proteins may serve analogous functions during latency of their respective viruses.

Introduction

Nuclear DNA is largely organized and controlled through nucleosomes. Each nucleosome typically assembles 146–147 base pairs (bp) of DNA in 1.65 superhelical turns around a core histone octamer composed of a central H3-H4 tetramer flanked by two H2A-H2B dimers (1, 2). Additionally, linker histone H1 binds to the nucleosome at the DNA entry-exit points outside the octamer. Thousands of nucleosomes along the DNA compose a "beads-on-a-string" array, which can further condense into higher order chromatin attaining its most compact state during mitosis (reviewed in 3, 4).

Herpesviruses transcribe, synthesize and package their double-stranded DNA genomes in the host cell nucleus where they contend with and exploit chromatin to aid viral replication and persistence. There are several examples of herpesvirus proteins interacting with cellular mitotic and/or interphase chromatin. The viral proteins attach to chromatin through at least three types of non-mutually exclusive molecular targets: DNA, histones, or chromatin-associated non-histone proteins. For instance, Epstein-Barr virus (EBV), a γ-herpesvirus, encodes the EBV nuclear antigen 1 (EBNA1) which targets host chromatin by interacting with adenosine/thymidine-rich DNA sequences (5) and EBNA1 binding protein 2 (6-9). In contrast, the latency-associated nuclear antigen 1 (LANA1 or LANA) encoded by another γ-herpesvirus, Kaposi's sarcoma-associated herpesvirus (KSHV), associates with chromatin through complex formation with non-histone factors including methyl CpG-binding protein (10) as well as with core histones H2A-H2B (11, 12) and, potentially, linker histone H1 (13). In fact, the crystal structure of a nucleosome complexed with the first 23 LANA amino acids revealed that the viral peptide forms a β-hairpin that specifically interacts with an "acidic pocket" formed by the folded regions of the

H2A-H2B dimer (12). Through chromatin interaction, LANA and other viral proteins assume fundamental roles in the infectious cycles of their respective viruses (see Discussion).

The 72-kDa immediate-early (IE) 1 protein (IE1-72kDa, IE72, or IE1) is a nuclear regulatory phosphoprotein of human cytomegalovirus (hCMV), the prototypic β-herpesvirus. IE1 is expressed from the hCMV genome at the onset of infection. Together with the 86-kDa IE2 protein (IE2-86kDa, IE86, or IE2), IE1 is the most prominent member of the major IE (MIE) family of hCMV gene products which have been assigned critical functions in virus-host interaction including innate immune modulation and transcriptional regulation (reviewed in 14-16). IE1 is required for viral early gene expression and replication in human fibroblasts, at least under conditions of low input multiplicity (17-19). Association of IE1 with condensed chromatin during mitosis was initially described more than 20 years ago (20) and has henceforward been conspicuous to many researchers (e.g., 21-28). The interaction with mitotic chromatin can be observed both during hCMV infection and upon ectopic expression of IE1. Chromosome association was first roughly mapped to MIE exon 4 sequences (20) and, subsequently, to residues 421 to 486 of the 491-amino-acid viral protein (24). Eventually, the 16 carboxy-terminal residues (amino acids 476 to 491) of IE1 were determined to be required and sufficient for mitotic chromatin interaction in transfected cells and were consequently termed the “chromatin tethering domain” (CTD) (22). The ability for chromosome attachment appears to be evolutionary conserved between IE1 orthologs of primate CMVs (21, 22, 29). However, despite being a conserved and distinctive feature of IE1, the mechanisms underlying chromosome association by the viral protein have not been determined.

90 The present study was designed to identify and precisely delineate the molecular
91 interactions anchoring the hCMV IE1 protein to human chromosomes, and to determine their
92 impact on viral replication in “clinical” strains of hCMV.

MATERIALS AND METHODS

Plasmids and mutagenesis. For expression in human cells, plasmid constructs derived from pcDNA3 (Life Technologies), pCGN (30), pCMV.TetO (a gift from Roger Everett, University of Glasgow, Scotland), pEGFP-C1 (Clontech), and pME18S (31) were used. For expression in *E. coli,* plasmid constructs derived from pGEX-KG (32) were used.

Plasmid pcDNA-HA-IE1 encodes the hCMV (Towne) 72-kDa IE1 (pUL123) protein tagged with an Influenza virus hemagglutinin (HA) epitope (21). Plasmid pcDNA-HA-mIE1 encodes an HA-tagged form of the mCMV IE1 (mIE1, pp89) protein and was constructed by inserting a *Bam*H1-*Eco*RI fragment from pGEX-mIE1 (21) into the same sites of pcDNA-HA-N (33) (a gift from Ronald Hay, University of Dundee, Scotland). For construction of pcDNA-HA-IE2, encoding an HA-tagged form of the hCMV 86-kDa IE2 (pUL122) protein, a *Bgl*II-*Eco*RI fragment from pEGFP-IE2 (21) was inserted into the *Bam*HI and *Eco*RI sites of pcDNA-HA-N. Plasmid pCGN-pp71 encodes an HA-tagged form of the hCMV pp71 (pUL82) protein (34). Plasmid pCMV.TetO.IE1 has been described (40). For pCMV.TetO.IE1M483A, pCMV.TetO.IE1NBM, and pCMV.TetO.IE1$_{1\text{-}475}$, mutant hCMV IE1 (Towne) coding sequences were PCR-amplified from template pEGFP-TNIE1 (21) with primers 483 and 1085, 483 and 1086, or 483 and 695, respectively, and inserted into the *Hin*dIII and *Eco*RI sites of pCMV-TetO. To generate pEGFP-IE1$_{476\text{-}491}$ and related constructs encoding the enhanced green fluorescent protein (EGFP) fused to the IE1 CTD or to CTD variants with single amino acid substitutions (G476A, G477A, K478A, S479A, T480A, M481A, P482A, M483A, V484A, T485A, R486A, S487A, K488A, A489G, D490A, and Q491A), suitable oligonucleotides (635–636 and 703–734) were annealed and inserted into the *Bgl*II and *Eco*RI sites of pEGFP-C1. A

116 construct replacing the first two IE1 coding triplets in pEGFP-IE1$_{476-491}$ with stop codons
117 (pEGFP-Stop) was generated in the same way using oligonucleotides 737 and 738. Likewise,
118 pEGFP-LANA$_{5-22}$ was generated by ligating annealed oligonucleotides 639 and 640 via *Bgl*II and
119 *Eco*RI sites with pEGFP-C1. All constructs expressing human histone H2A (H2A.2, type 1-B/E)
120 were based on pME-Flag-H2A (35) (a gift from Robert Eisenman, Fred Hutchinson Cancer
121 Research Center, Seattle, USA). To generate constructs encoding Flag-tagged H2A with single
122 (E41A, E56A, E61A, E64A, D72A, D90A, E91A, E92A, and E121A) and triple
123 (E61A/E64A/D90A and D90A/E91A/E92A) amino acid substitutions, QuikChange site-directed
124 mutagenesis (Stratagene) was performed according to the manufacturer's instructions using
125 suitable oligonucleotides (787–808).

126 In pGEX-KG, the *Bam*HI and *Eco*RI sites served for all cloning reactions. Plasmid
127 pGEX-IE1 encodes the hCMV (Towne) 72-kDa IE1 protein fused to GST (21). To generate
128 pGEX-IE1$_{1-475}$, a PCR product amplified from template pGEX-IE1 with primers 637 and 638 was
129 digested with *Bam*HI and *Eco*RI and ligated with pGEX-KG. For construction of pGEX-IE1$_{476-491}$ and related constructs encoding GST fused to the IE1 CTD or to CTD variants with single
131 amino acid substitutions, suitable oligonucleotides (635–636 and 703–734) were annealed and
132 ligated with pGEX-KG. A construct replacing the first two IE1 coding triplets in pGEX-IE1$_{476-491}$
133 with two stop codons (pGEX-Stop) was generated in the same way using oligonucleotides 737
134 and 738. Likewise, pGEX-LANA$_{5-22}$ was generated by ligating annealed oligonucleotides 639
135 and 640 with pGEX-KG. To construct pGEX-PreS-IE1, a DNA fragment encoding the
136 recognition motif for PreScission Protease (LEVLFQGP) between the GST and IE1 sequences
137 was generated by overlap extension PCR (36) from templates pGEX-KG and pGEX-IE1 with
138 primers 484 and 603–605. The PCR product was digested with *Bam*HI and *Eco*RI and ligated
139 with pGEX-IE1. Plasmid pGEX-PreS-IE1 was used as a template for PCR with primers 695 and

838 resulting in a DNA fragment that was digested with *Bam*HI and *Eco*RI and ligated with pGEX-PreS-IE1 to produce pGEX-PreS-IE1$_{1-475}$. Finally, pGEX-PreS-IE1$_{476-491}$, pGEX-PreS-LANA$_{5-22}$, and pGEX-PreS were generated by ligating annealed oligonucleotides 834 and 835, 836 and 837, or 658 and 659, respectively, with pGEX-PreS-IE1.

As a standard for absolute quantification of hCMV genome copies by real-time quantitative PCR (qPCR), plasmid pCR-RPPH1-UL54P was constructed by a two-step procedure. First, a PCR product comprising 71 bp of hCMV UL54 promoter (UL54P) sequence was amplified from an infected cell genomic DNA template with primers 294 and 295, and was ligated with pCR4-TOPO (Life Technologies). Secondly, the resulting construct (pCR-UL54P) was cleaved with *Pme*I and ligated with a PCR product comprising 83 bp of human ribonuclease P RNA component H1 (RPPH1) sequence amplified from an infected cell genomic DNA template with primers 759 and 765. All oligonucleotide sequences are listed in Table S1.

Cells, viruses, and infections. Human fetal diploid lung fibroblasts (MRC-5) (37) were obtained from the European Collection of Cell Cultures, and early-passage cells (15 to 25 population doublings before senescence) were used in all experiments. MRC-5-derived TetR cells and TetR-IE1 cells expressing inducible wild-type IE1 have been described (40). TetR-IE1$_{1-475}$ cells expressing inducible CTD-deleted IE1 were generated via lentiviral transduction analogous as described for TetR-IE1 cells (40). The H1299 human lung carcinoma cell line (38) was obtained from the American Type Culture Collection. MRC-5 and H1299 cells were grown in Dulbecco's Modified Eagle's Medium (DMEM) (Life Technologies) supplemented with 10% fetal calf serum (Life Technologies), 100 U/ml penicillin, and 100 µg/ml streptomycin. For TetR, TetR-IE1, and TetR-IE1$_{1-475}$ cells, the same medium was further supplemented with 1 µg/ml puromycin and 300 µg/ml G418, and induction of IE1 or IE1$_{1-475}$ expression was accomplished

by adding doxycycline (1 µg/ml) 72 h prior to collection. All cells were maintained under humidified conditions at 37°C and 5% CO_2. Cultures were regularly screened for mycoplasma contamination.

The wild-type (TNwt) and IE1-deficient (TNdlIE1) viruses of the high passage hCMV Towne strain (39) were described previously (21, 40, 41). The wild-type (TBwt) virus of the low passage hCMV TB40E strain (42) was derived from TB40-BAC4 (43) (a gift from Christian Sinzger, Ulm University, Germany). For the construction of TB40E-based IE1 CTD-deficient bacterial artificial chromosomes (BACs) (pTBIE1$_{1\text{-}475}$) by *en passant* mutagenesis, *E. coli* strain GS1783 (44) carrying TB40-BAC4 was transformed with a *Dpn*I-digested and column-purified PCR product generated using plasmid pLAY2 (45) (a gift from Karsten Tischer, Freie University Berlin, Germany) as a template and oligonucleotides 870 and 871 as primers. "Scarless" removal of CTD-specific sequences by homologous recombination was accomplished following published protocols (44). To control for inadvertent genetic changes, the *en passant* strategy was also employed to construct "revertant" BACs (pTBrvIE1$_{1\text{-}475}$). To this end, a PCR product comprising MIE exon 4 was generated using TB40-BAC4 as a template and oligonucleotides 876 and 877 as primers. This PCR product was inserted into pUC18 via *Hin*dIII and *Eco*RI sites resulting in plasmid pUC-MIE. In addition, a PCR product comprising a kanamycin resistance (*kan*) cassette and an *Sce*I cleavage site was generated, using pLAY2 as a template and oligonucleotides 878 and 879 as primers. Following cleavage with *Nco*I, this PCR product was inserted into the *Nco*I site of pUC-MIE resulting in plasmid pUC-MIE-*kan_Sce*I. Then, GS1783 bacteria carrying BAC pTBIE1$_{1\text{-}475}$ were transformed with a *Dpn*I-digested and column-purified PCR product generated using plasmid pUC-MIE-*kan_Sce*I as a template and oligonucleotides 880 and 881 as primers, and this was followed by homologous recombination (44). The identity and integrity of pTBIE1$_{1\text{-}}$

187 $_{475}$ and pTBrvIE1$_{1\text{-}475}$ were verified in comparison to TB40-BAC4 by restriction fragment length
188 and DNA sequencing analyses (data not shown).

189 Allelic exchange to generate IE1 CTD-deficient (pFXIE1$_{1\text{-}475}$) and revertant (pFXrvIE1)
190 BACs of the low passage hCMV FIX strain (46, 47) utilized the following derivatives of transfer
191 plasmid pGS284 (48) (amplified in *E. coli* strain S17λpir): pGS284-FXIE1*kanlac*Z, pGS284-
192 FXMIE, and pGS284-FXIE1$_{1\text{-}475}$. Plasmid pGS284-FXIE1*kanlac*Z contains the *kan* and *lacZ*
193 genes cloned between sequences flanking the IE1-specific exon four of the hCMV FIX MIE
194 transcription unit. The ~1,000-bp flanking sequences were obtained by PCR amplification using
195 primers 136 and 138 (downstream flanking sequence) or 139 and 140 (upstream flanking
196 sequence), and an EGFP expressing hCMV FIX BAC (pFXwt) (a gift from Dong Yu,
197 Washington University School of Medicine, USA) as template. The amplified downstream
198 flanking sequence was cloned into pGS284 via *Bgl*II and *Not*I sites. Following addition of
199 adenosine nucleotide overhangs to the PCR product, the upstream flanking sequence was first
200 subcloned into vector pCR4-TOPO (Life Technologies) and subsequently inserted via *Not*I sites
201 into pGS284 carrying the downstream flanking sequence. The *kanlac*Z expression cassette was
202 released from plasmid pGEM-*kanlacZ* (YD-C54) (49) and cloned into the *Pac*I site located
203 between the hCMV flanking sequences in the pGS284 derivative described above. For the
204 construction of pGS248-FXMIE, a ~3,000-bp sequence of the MIE region was amplified by PCR
205 using template pFXwt and primers 155 and 156. After phosphorylation, the PCR product was
206 first inserted into the *Sma*I site of pUC18 to generate pUC18-FXMIE. Plasmid pUC18-FXMIE
207 served as a template for QuikChange site-directed mutagenesis with oligonucleotides 280 and
208 281 replacing IE1 codon 475 with a stop codon to generate pUC18-FXIE1$_{1\text{-}475}$. Then, *Fse*I-*Not*I
209 fragments were excised from pUC18-FXMIE and pUC18-FXIE1$_{1\text{-}475}$ and cloned into the same

sites of pGS284-FXIE1*kanlac*Z thereby generating pGS284-FXMIE and pGS284-FXIE1$_{1\text{-}475}$, respectively. For verification, DNA sequence analysis was completed on all cloned PCR amplification products. Allelic exchange was performed through homologous recombination in *E. coli* strain GS500 as previously described (21, 48, 49). First, the BAC pFXIE1*kanlac*Z was generated by recombination of pFXwt with pGS284-FXIE1*kanlac*Z followed by selection for kanamycin resistance and LacZ expression. After that, the BACs pFXIE1$_{1\text{-}475}$ and pFXrvIE1 were made through recombination of pFXIE1*kanlac*Z with pGS284-FXIE1$_{1\text{-}475}$ and pGS284-FXMIE, respectively, followed by selection for the loss of kanamycin resistance and LacZ expression. The identity and integrity of pFXIE1$_{1\text{-}475}$ and pFXrvIE1 were verified in comparison to pFXwt by restriction fragment length and DNA sequence analyses (data not shown). All oligonucleotide sequences are listed in Table S1.

Cell- and serum-free virus stocks were produced upon electroporation of MRC-5 cells with BAC clones carrying wild-type (TNwt, FXwt, TBwt), revertant (FXrvIE1, TBrvIE1$_{1\text{-}475}$), or IE1 CTD-deficient (FXIE1$_{1\text{-}475}$, TBIE1$_{1\text{-}475}$) genomes. Stocks of TNdlIE1 viruses were produced in a similar fashion, following electroporation of TetR-IE1 cells (40). All virus stocks were screened for mycoplasma contamination. Titers were calculated by qPCR-based absolute quantification of intracellular viral genome copies following infection of MRC-5 cells as described (21, 40) and by comparing the results to a standard curve based on amplifications from plasmid pCR-RPPH1-UL54P (see above) mixed with salmon sperm DNA. For wild-type viruses, titers were also determined by standard plaque assay on MRC-5 cells. For mutant and revertant viruses, plaque forming units relative to wild-type titers were calculated from intracellular viral copy numbers. Infections were carried out at the indicated input multiplicities and for the indicated durations on (nearly) confluent MRC-5 cells.

Protein production, purification, and analysis. For protein production in *E. coli,* a single colony of the Rosetta strain (Novagen) transformed with pGEX-KG or derivatives was grown by shaking (220 revolutions per minute [rpm]) overnight at 28°C in Luria-Bertani medium containing ampicillin (50 µg/ml), chloramphenicol (20 µg/ml), and 2% glucose. On the next day, the culture was diluted to an optical density at 600 nm (OD_{600}) of 0.1 with fresh prewarmed medium lacking glucose and further grown for 2–3 h at 220 rpm and 28°C to an OD_{600} of 0.6. At this point, gene expression was induced by adding isopropyl-β-D-thiogalactopyranoside to a final concentration of 200 µM. Following a 6-h incubation at 220 rpm and 28°C, cells were quick-chilled on ice and collected by centrifugation (~2,500×g, 15 min, 4°C). Bacteria were resuspended in 1/10 culture volume ice-cold wash buffer (50 mM Tris-HCl [pH 7.5], 150 mM NaCl, 2 mM $MgCl_2$, 1 mM DTT, cOmplete EDTA-free Protease Inhibitor Cocktail [Roche]). After another round of centrifugation (~2,500×g, 15 min, 4°C), the pellet was resuspended in 1/25 culture volume ice-cold wash buffer containing 1 mM phenylmethylsulfonyl fluoride (added freshly). The suspension was snap-frozen in liquid nitrogen and stored at -80°C.

To purify GST and GST fusion proteins, bacteria suspended in wash buffer (see above) were thawed in a water bath at room temperature. For the subsequent workflow, ice-cold buffers and solutions were used, and all steps were carried out on ice or at 4°C. Following addition of lysozyme (150 µg/ml) and benzonase (25 U/ml), the suspension was sonicated five times for 1 min using a Branson Sonifier 450 (duty cycle 80%, output control 2) to facilitate cell lysis. The lysate was combined with 1/9 volume wash buffer containing 10% Triton X-100, rotated for 30 min to solubilize proteins, and centrifuged (20,000×g, 30 min). The affinity matrix was prepared by washing Glutathione Sepharose 4B (GE Healthcare) consecutively in ten bed volumes equilibration buffer (50 mM Tris-HCl [pH 7.5], 150 mM NaCl, 2 mM $MgCl_2$), 10 bed volumes blocking buffer (equilibration buffer with 2% bovine serum albumin) (1 h under rotation), and

another 10 volumes equilibration buffer. After that, 1.25 ml equilibrated matrix per 1,000 ml culture volume and the supernatant from the bacterial lysate were combined and rotated for 2 h. The sample was then applied to a 10-ml Pierce Centrifuge Column (Thermo Scientific), and the matrix was washed consecutively with 50 bed volumes low salt wash buffer (50 mM Tris-HCl [pH 7.5], 150 mM NaCl, 1 mM dithiothreitol [DTT], 1% Triton X-100, 1 mM EDTA, cOmplete EDTA-free Protease Inhibitor Cocktail), 50 bed volumes high salt wash buffer (50 mM Tris-HCl [pH 7.5], 500 mM NaCl, 1 mM DTT, 1% Triton X-100, 1 mM ethylenediaminetetraacetic acid (EDTA), cOmplete EDTA-free Protease Inhibitor Cocktail), and another 50 bed volumes low salt wash buffer. After the final washing step, one bed volume low salt wash buffer was added, the column was sealed, and the 50% slurry containing purified proteins was stored in ice until use. To remove the GST tag from GST-IE1 and GST-$IE1_{1\text{-}475}$, the protein-loaded matrix was washed with 50 bed volumes cleavage buffer (PBS with 1 mM DTT), the column outlet was sealed, and one bed volume of cleavage buffer containing PreScission protease (50 U/ml, GE Healthcare) was added. Protein cleavage was allowed to proceed in the sealed column for 16 h under rotation. After that, the flow-through containing IE1 or $IE1_{1\text{-}475}$ proteins was collected. Protein concentrations were calculated assuming absorption at 280 nm values of 0.396 or 0.409 for 1 g/1,000 ml (0.1%) IE1 or $IE1_{1\text{-}475}$, respectively.

For preparation of nucleosomes, H1299 cells grown to confluency were scraped on ice and collected in 15-ml tubes by centrifugation (500×g, 5 min, 4°C). For the subsequent workflow, ice-cold buffers and solutions were used, and all steps were carried out on ice or at 4°C. Cell pellets, each corresponding to one 10-cm plate, were resuspended in 1 ml MNase lysis buffer (10 mM Tris-HCl [pH 7.4], 10 mM NaCl, 3 mM $MgCl_2$, 150 µM spermine, 500 µM spermidine, 0.5% IGEPAL CA-630) and vortexed while simultaneously adding another 4 ml MNase lysis buffer. Following a 5-min incubation, samples were centrifuged (300×g, 5 min), the supernatant

was removed completely, and nuclei were washed in 500 µl MNase reaction buffer (10 mM Tris-HCl [pH 7.4], 15 mM NaCl, 60 mM KCl, 150 µM spermine, 500 µM spermidine). After that, nuclei were carefully resuspended in 100 µl MNase reaction buffer with 1 mM $CaCl_2$ and prewarmed for exactly 5 min at 30°C. Extra-nucleosomal DNA was digested by adding 100 U Nuclease S7 MNase from *Staphylococcus aureus* (Roche) diluted in MNase dilution buffer (5 mM Tris-HCl [pH 7.4], 10 µM $CaCl_2$). Following incubation for 10 min at 30°C, reactions were stopped with 20 mM EDTA and 2 mM ethylene glycol tetraacetic acid. For co-immunoprecipitations, nucleosome preparations (120 µl) were combined with whole cell extracts prepared as described above.

Histones were purified by acid extraction from H1299 cell nuclei. Cells grown to confluency were scraped on ice and collected in 15-ml tubes by centrifugation (500×g, 5 min, 4°C). For the subsequent workflow, ice-cold buffers and solutions were used, and all steps were carried out on ice or at 4°C. Cell pellets, each corresponding to one 15-cm plate, were resuspended in 1 ml hypotonic lysis buffer (10 mM Tris-HCl [pH 7.5], 10 mM NaCl, 3 mM $MgCl_2$, 10 mM DTT, 0.5% IGEPAL CA-630, EDTA-free Protease Inhibitor Cocktail Set III). Then, 4 ml hypotonic lysis buffer were added while samples were concomitantly vortexed at medium speed. Following a 5-min incubation, nuclei were collected by centrifugation (500×g, 5 min) and washed by repeating the consecutive 1-ml and 4-ml resuspension steps in hypotonic lysis buffer twice (without the 5-min incubation in between). Following centrifugation (500×g, 1 min), the supernatant was removed completely, the pellet was resuspended in 1 ml 200 mM H_2SO_4, and the nuclei were transferred to 1.5-ml tubes. After that, samples were incubated for 16 h on a rotator. Following extraction, samples were centrifuged (20,000×g, 30 min) to remove insoluble debris, and 900 µl supernatant were transferred to a new 1.5-ml tube. Histones were precipitated by addition of trichloroacetic acid (TCA) to a final concentration of 35% and

overnight incubation at -20°C. After centrifugation (20,000×g, 15 min), the protein pellet was washed by sonication (Branson Sonifier 450; 10 pulses, duty cycle 80%, output control 8) in 1 ml acetone with 50 mM HCl and, subsequently, in 1 ml pure acetone at room temperature. After a final centrifugation step (20,000×g, 15 min), pellets were dried at room temperature. For binding assays, histones were resuspended in an appropriate volume of reaction buffer by sonication (Branson Sonifier 450; 10 pulses, duty cycle 80%, output control 8) and repeated pipetting.

For separation of histones into fractions containing either H2A-H2B or H3-H4, the purification protocol was extended by an ion exchange chromatography step (50) following acid extraction. Briefly, a 2-ml Pierce Centrifuge Column was filled with 1 ml Sulfopropyl-Sepharose Fast Flow (Sigma-Aldrich) and washed twice with 8.1 ml wash buffer I (50 mM Tris-HCl [pH 8.0], 200 mM NaCl, 2 mM EDTA). Concurrently, histone extracts (prepared as described above) from six 15-cm dishes of H1299 cells were pooled in a 50-ml tube and combined with 2 volumes of 1 M Tris-HCl (pH 8.0). After verifying the pH (pH 7.0–8.0), 200 mM NaCl, 1 mM DTT, and 2 mM EDTA were added, and the mixture was applied to the filled column. The column was washed with 8.1 ml wash buffer II (50 mM Tris-HCl [pH 8.0], 500 mM NaCl, 2 mM EDTA [pH 8.0]) and, subsequently, with the same volume of wash buffer III (50 mM Tris-HCl [pH 8.0], 600 mM NaCl, 2 mM EDTA). For elution of H2A-H2B, 6.6 ml elution buffer I (50 mM Tris-HCl [pH 8.0], 800 mM NaCl, 2 mM EDTA) were added to the column, of which the first 600 µl were discarded and six 1-ml fractions were collected. Following two 8.1-ml wash steps with elution buffer I, H3-H4 was eluted with 2.5 ml elution buffer II (50 mM Tris-HCl [pH 8.0], 2 M NaCl, 2 mM EDTA) and collected in five 500 µl-fractions. A subset of histone fractions (determined by polyacrylamide-sodium dodecyl sulfate [SDS] gel electrophoresis and Coomassie Brilliant Blue staining, see below) were pooled and subjected to TCA precipitation as described above.

For protein analysis, samples were mixed with 2×loading buffer (100 mM Tris-HCl [pH 6.8], 4% SDS, 20% glycerol, 0.2% bromphenol blue, 200 mM β-mercaptoethanol), denatured for 5 min at 95°C, and separated in SDS-polyacrylamide gels that were either stained with Coomassie Brilliant Blue (PlusOne Coomassie Blue PhastGel R-350, GE Healthcare) according to the manufacturer's instructions, or subjected to immunoblotting including chemiluminescent detection (SuperSignal West Pico or SuperSignal West Femto, Thermo Scientific) as described (51). The following antibodies were used for protein detection following blotting: α-Flag (M2, Sigma-Aldrich), α-GAPDH (ab9485, Abcam), α-HA (3F10, Roche), α-H2A (ab13923, Abcam), α-H2B (ab1790, Abcam), α-H3 (ab1791, Abcam), α-H4 (62-141-13, Upstate), α-IE1 (1B12, [52]; ab30924 [IE1.G10], Abcam; 6E1, Santa Cruz), α-IE1/IE2 (MAB810R, Merck Millipore), and horseradish peroxidase-coupled anti-mouse (115-036-003, Dianova), anti-rabbit (AP156P, Chemicon), or anti-rat (112-035-003, Dianova) secondary conjugates.

Protein binding and competition analysis. For co-immunoprecipitations, subconfluent H1299 cells on 10-cm plates were transfected with 10 μg plasmid DNA using a calcium phosphate precipitation technique (53). Approximately 48 h post transfection, cells were stored at room temperature for 10 min and cross-linked by adding formaldehyde to a final concentration of 1% directly to the medium. Following a 5-min incubation at room temperature, a glycine solution (125 mM final concentration) was added to each dish to terminate cross-linking. After another 5-min incubation at room temperature, the medium was removed, and cells were washed twice with 10 ml ice-cold serum-free DMEM. For the subsequent workflow, ice-cold buffers and solutions were used, and all steps were carried out on ice or at 4°C. Cells were scraped into 2 ml serum-free DMEM with EDTA-free Protease Inhibitor Cocktail Set III (Merck Millipore), and each dish

was washed three times with 2.5 ml serum-free DMEM for optimal cell recovery. After that, cells were centrifuged (2,500×g, 10 min), and the medium was removed completely. The cell pellet was resuspended in 1 ml immunoprecipitation (IP) lysis buffer (50 mM Tris-HCl [pH 7.5], 125 mM NaCl, 500 µM DTT, 0.5% IGEPAL CA-630, 1% Triton X-100, 5 mM EDTA, EDTA-free Protease Inhibitor Cocktail Set III), and the suspension was incubated for 5 min. After centrifugation (12,000×g, 1 min), the pellet was washed in IP lysis buffer, recentrifuged (12,000×g, 1 min), resuspended in IP lysis buffer, and incubated for 10 min. Then, the cell lysate was sonicated three times for 5 min in a Bioruptor UCD-200 (Diagenode; position "H", 30 s on-off cycle) to shear the chromatin. After that, insoluble debris was removed by centrifugation (20,000×g, 30 min), and 900 µl supernatant were transferred to a new 1.5-ml tube. The following matrices were used for the subsequent immunoprecipitation reactions: Anti-Flag M2 Affinity Gel (Sigma-Aldrich), Monoclonal Anti-HA-Agarose (HA-7, Sigma-Aldrich), Mouse IgG-Agarose (Sigma-Aldrich), or Protein A Agarose/Salmon Sperm DNA (Merck Millipore). Before use, agarose beads were washed three times in 1 ml IP lysis buffer. To preclear the lysate, 100 µl (20 µl bed volume) Mouse IgG-Agarose or Protein A Agarose/Salmon Sperm DNA were added, and the mixture was rotated for 1 h. Following centrifugation (20,000×g, 30 min), 50 µl supernatant were removed to serve as input sample and 850 µl were transferred to a new 1.5-ml tube. For reactions using Protein A Agarose/Salmon Sperm DNA, the lysate was incubated overnight with α-H3 antibodies (ab1791, Abcam) or IgG from rabbit serum (Sigma-Aldrich). Then, 100 µl (20 µl bed volume) of the respective antibody-coupled or Protein A agarose matrix were added. After rotation for 1 h, samples were centrifuged (100×g, 1 min), and the supernatant was removed completely. The protein-loaded matrix was resuspended in 100 µl DNase buffer (Ambion) and reacted with 2 µl (4 U) DNase I (Ambion) for 15 min at 25°C. After that, 1 ml IP lysis buffer was

added, and the matrix was washed five times in the same buffer. Following the final centrifugation step (100×g, 1 min), the pellet was resuspended in 45 µl 1×loading buffer, and samples were heated (10 min for output and 5 min for input samples). Before electrophoresis, output samples were centrifuged (16,000×g, 5 min), and only the supernatant was used for immunoblotting.

For GST pull-down assays, ice-cold buffers and solutions were used, and all steps were carried out on ice or at 4°C. For each reaction, 20 µl (bed volume) Glutathione Sepharose 4B (GE Healthcare) loaded with GST or GST fusion proteins were washed twice in 700 µl binding buffer (50 mM Tris-HCl [pH 8.0], 150 mM NaCl, 1 mM DTT, 10% glycerol, 0.5% Triton X-100, EDTA-free Protease Inhibitor Cocktail Set III). Acid-extracted histones from one half 15-cm dish of H1299 cells in 300 µl binding buffer were subjected to one 10 min and two 5 min centrifugations (20,000×g) to remove insoluble debris. The histone solution was subsequently combined with the washed protein-loaded sepharose matrix, and 10% of the total volume was removed to serve as input sample. The suspension was rotated for 90 min to facilitate binding. After that, the matrix was washed five times in 700 µl binding buffer, resuspended in 100 µl 1×loading buffer, heated, and analyzed.

To analyze competition between IE1 and LANA for nucleosome/histone binding, synthetic peptides encompassing KSHV LANA residues 5 to 22 (LANA-CTD: GMRLRSGRSTGAPLTRGS) or a mutant amino acid sequence deficient for histone binding (LANA-CTD*: GMRAAAGRSTGAPLTRGS) were purchased from Thermo Scientific and dissolved in water. IE1 and $IE1_{1-475}$ proteins were derived from the respective GST fusion proteins by cleavage with PreScission protease (GE Healthcare). Acid-extracted histones in binding buffer were preincubated for 1 h with various concentrations of LANA-CTD or LANA-CTD* (1 mM stock solution), IE1 (95 µM stock solution), or $IE1_{1-475}$ (83 µM stock solution).

399 After that, the samples were centrifuged (20,000×g, 15 min), and the supernatant was reacted
400 with the respective GST or GST fusion proteins coupled to Glutathione Sepharose 4B as
401 described above.
402 For protein quantification, bands were scanned at 72 dots per inch and subjected to
403 densitometry using Scion Image 4.0.2 software (Scion Corporation) including the GelPlot2
404 extension.
405
406 **Immunofluorescence and microscopy.** Subconfluent H1299 or MRC-5 cells grown on
407 sterile coverslips in 6-well dishes were transfected with 5 µg plasmid DNA using a calcium
408 phosphate precipitation technique (53). Alternatively, MRC-5 cells were mock- or hCMV-
409 infected as described in Supplemental Material. Approximately 48 h post transfection or
410 infection, cells were washed three times with phosphate-buffered saline (PBS) containing 0.05%
411 Tween 20 (PBS-T) and fixed with ice-cold methanol for 20 min at -20°C. After three 5-min
412 washes with PBS-T, samples were blocked for 1 h in PBS-T containing 2% bovine serum
413 albumin (BSA) and reacted for 1 h with the respective primary antibodies in a humidity chamber.
414 The primary antibodies used for immunofluorescence were α-EGFP (ab290, Abcam) or α-IE1
415 (ab30924 [IE1.G10], Abcam; sc-69834 [6E1], Santa Cruz). Following three 5-min washes with
416 PBS-T and a 1-h incubation with the appropriate Alexa Fluor 488- and Alexa Fluor 594-
417 conjugated secondary antibodies (Life Technologies) and 0.2 µg/ml 4′,6-diamidino-2-
418 phenylindole (DAPI) (Roche), coverslips were mounted on glass slides using ProLong Gold (Life
419 Technologies). Slides were analyzed using a Keyence BZ 9000 (Generation II) or a Leica DMRX
420 epifluorescence microscope equipped with a digital camera system (Retiga, Q-Imaging), and
421 images were acquired and processed using BZ II Analyzer (Keyence) or Image-Pro Plus (version

6.2) (Q-Imaging) and Adobe Photoshop CS4 software. The extent of overlap between pixels in the green and blue channels was quantified by calculating Pearson's correlations from autocontrasted eight bit images using ImageJ software (National Institutes of Health) and the Colocalization_Finder (version 1.2) plugin (http://rsb.info.nih.gov/ij/plugins/colocalization-finder.html).

Molecular modeling. Homology modeling was performed using the PERMOL module (54) implemented in the AUREMOL package (55). The 16 carboxy-terminal residues (amino acids 476–491) of hCMV (Towne) IE1 were aligned with 14 amino-terminal residues (amino acids 4–17) of KSHV LANA using a program based on the Needleman-Wunsch algorithm contained in PERMOL. The alignment was confirmed with other programs including ClustalW2 (http://www.ebi.ac.uk/tools/msa/clustalw2) and EMBOSS Stretcher (http://www.ebi.ac.uk/tools/psa/emboss_stretcher), respectively. An alternative alignment was produced by just one of all tested programs (LALIGN; http://www.ebi.ac.uk/tools/psa/lalign). Other possible alignments were excluded as they did not involve the nucleosome binding motif (GMRLRSG) of the LANA CTD. As a template for homology modeling, we used the x-ray structure of the $LANA_{4-17}$-nucleosome complex (12) (PDB: 1zla). The modeling was restricted to the interaction site of the LANA peptide with histones H2A and H2B, i.e., LANA amino acids 4–17, H2A amino acids 14–107, and H2B amino acids 30–122 could evolve using restrained molecular dynamics while the remaining part of the histone complex was held rigid during the calculations. For the modeling, the LANA peptide was replaced by the IE1 CTD using either of the two reasonable amino acid sequence alignments. In a second step, we used PERMOL to generate interatomic distance restraints, dihedral angle restraints, and hydrogen bonds from the H2A-H2B/IE1 CTD model template based on the degree of sequence conservation between the

LANA and IE1 CTDs. With this set of restraints, 1,000 structures were calculated per each model using the molecular dynamics program Crystallography & NMR System (56, 57). The twenty best structures in terms of total energy were used for explicit water refinement (58). After the water refinement, a bundle of the ten lowest energy structures was selected for each of the two models.

RESULTS

IE1 interacts with nucleosomes in a nucleic acid-independent fashion. We started the work by employing immunoprecipitation-immunoblotting analysis to investigate whether IE1 and other nuclear localized CMV proteins are physically associated with nucleosomes. For the first set of binding assays, extracts from cells transfected either with empty vector or with plasmids encoding epitope-tagged hCMV IE1, murine cytomegalovirus (mCMV) IE1 (mIE1), hCMV IE2, and hCMV pp71 were combined with exogenous nucleosomes prepared by micrococcal nuclease (MNase) digestion of human cell nuclei. Readily detectable amounts of core histones from all four classes (H2A, H2B, H3, and H4) were found to co-precipitate with IE1, while much smaller amounts were detected with IE2. Very little, if any, histone binding was observed in the mIE1, pp71, and empty vector transfections. Likewise, a non-specific antibody did not precipitate any appreciable amounts of core histones (Fig. 1A). In a second round of experiments, we checked for co-precipitation of endogenous nucleosomes solubilized by sonication with epitope-tagged IE1, mIE1, IE2, and pp71. Under these conditions, specific core histone binding could only be demonstrated for IE1, but not for any of the other viral proteins under investigation (Fig. S1). Importantly, IE1 was found to specifically interact with endogenous core histones not only in plasmid-transfected but also in hCMV-infected cells (Fig. 1B).

To confirm the results obtained by immunoprecipitation-immunoblotting in another type of binding assay, we expressed IE1 fused to glutathione S-transferase (GST) in *Escherichia coli* and affinity-purified the protein on glutathione sepharose beads. GST-IE1 beads and beads loaded with only GST or no protein (empty beads) were subsequently reacted with acid-extracted histones, and samples were analyzed by electrophoresis in polyacrylamide gels stained with

Coomassie Brilliant Blue. The four core histones were found to interact with GST-IE1 at an approximately equimolar ratio, while only minor binding to GST or empty beads was observed in these assays (Fig. 1C). IE1 is not believed to bind DNA or RNA directly, and acid-extracted histone preparations are not supposed to contain intact nucleic acids. However, to fully rule out the possibility that the observed IE1-histone interactions are mediated through DNA or RNA, the pull-down assays were repeated in the presence of excess amounts of nucleases (DNase I and RNase A). As expected, the results obtained from DNase- and RNase-treated samples were virtually indistinguishable from those obtained in the absence of nucleases (Fig. 1C).

Taken together, the results from our *in vivo* and *in vitro* interaction assays demonstrate that IE1 specifically binds to human nucleosome cores, most likely through direct interaction with histones.

IE1 interacts with core histones via two separable regions with distinct binding specificities. To investigate whether core histones interact with IE1 residues previously shown to be required for chromosome association (22), we constructed plasmids encoding GST fused either to a carboxy-terminally truncated IE1 lacking the CTD (GST-IE1$_{1-475}$) or to an amino-terminally truncated IE1 consisting of only the CTD (GST-IE1$_{476-491}$). We also generated a plasmid encoding GST fused to the KSHV LANA amino-terminal CTD (GST-LANA$_{5-22}$) (59, 60), which was shown to bind to the H2A-H2B dimer of the nucleosome (12, 61) (Fig. 2A). Following expression in *E. coli,* the GST fusion proteins were used in pull-down assays with acid-extracted histone preparations as described above for wild-type GST-IE1 (see Fig. 1C). With GST-IE1$_{1-475}$, a reduction in H2A and H2B binding was evident compared to the full-length protein, whereas H3 and H4 binding was not negatively affected. Conversely, GST-IE1$_{476-491}$ and GST-LANA$_{5-22}$ did not specifically interact with H3 and H4. Instead, both GST-IE1$_{476-491}$ and

GST-LANA$_{5-22}$ displayed selective affinity for H2A and H2B. The interaction between H2A-H2B and GST-IE1$_{476-491}$ was less efficient compared to full-length GST-IE1, but about equally efficient compared to GST-IE1$_{1-475}$ and GST-LANA$_{5-22}$. No interaction between any of the GST proteins and linker histone H1 was detected (Fig. 2B). Notably, CTD-mediated complex formation between IE1 and H2A or H2B was also observed in co-immunoprecipitations from cells arrested in interphase (G0 phase), indicating that nucleosome targeting by the viral protein is not restricted to mitosis (Fig. S2).

To discriminate between direct and indirect core histone interactions, acid-extracted histones were further purified and separated into fractions highly enriched for either H2A-H2B dimers or H3-H4 dimers/tetramers. As predicted from the preceding experiments (see Fig. 2B), GST-IE1$_{1-475}$ and GST-IE1$_{476-491}$ displayed H2A-H2B binding comparable to GST-LANA$_{5-22}$ but less efficient compared to full-length GST-IE1. By contrast, GST-IE1 and GST-IE1$_{1-475}$ were equally efficient in binding to H3-H4. Finally, for GST-IE1$_{476-491}$ and GST-LANA$_{5-22}$ no H3-H4 interaction above background was observed (Fig. 2C).

The results from these experiments allow for several conclusions: (i) IE1 binds to core histones through at least two physically separable (and therefore independent) interaction surfaces, i.e., the CTD and unspecified sequences located upstream from the carboxy-terminus; (ii) the CTD selectively binds to H2A-H2B dimers through direct interaction, while the upstream histone binding domain directly binds to both H2A-H2B and H3-H4 dimers/tetramers with a preference for H3-H4; (iii) there are striking similarities between nucleosome binding by the IE1 and LANA CTDs.

Alanine scanning mutagenesis identifies a discrete nucleosome binding motif within the IE1 CTD. To gain further insight into the physical requirements of IE1-nucleosome complex

formation, we decided to determine which individual CTD residues contribute to the interaction. For this purpose, we performed alanine scanning mutagenesis replacing each of the 16 amino acids comprising the IE1 CTD with alanine (except for A489, which was replaced by glycine) (Fig. 3A). All mutant CTDs were expressed as GST fusion proteins in *E. coli* and used in pull-down assays with acid-extracted histones. The IE1 CTD pulled down all four core histones in these assays, most likely because the experimental conditions (i.e., higher histone concentrations leading to a larger proportion of octamers compared to Fig. 2B) allowed not only for direct (H2A-H2B) but also for indirect (H3-H4) interactions. Again, no binding to linker histone H1 was observed. Interestingly, only four CTD residues (H481, M483, T485, and R486) proved to be essential for histone binding. In addition, six amino acids (S479, T480, P482, V484, S487, and K488) turned out to augment the interaction significantly. In contrast, mutation of all residues upstream of S479 (G476, G477, and K478) and downstream of K488 (A489, D490, and Q491) had no obvious adverse effect on CTD-histone complex formation. In fact, the D490A exchange appeared to even enhance histone binding compared to the wild-type CTD (Fig. 3B–C).

In order to link the *in vitro* histone binding results to cellular chromosome association, we also expressed the wild-type and mutant CTD peptides as fusion proteins with amino-terminal EGFP in human cells. Co-staining of the EGFP-CTD proteins with mitotic DNA revealed that each of the same four residues shown to be essential for histone binding (H481, M483, T485, and R486) is also indispensable for chromosome attachment (Fig. 4A□B). Alanine substitution of all four essential CTD residues or individual substitution of M483 also abolished mitotic chromatin association of IE1 in the context of the full-length protein (Fig. 4C). Moreover, in agreement with the binding results, individual exchange of S479, T480, P482, V484, S487, and K488 was linked to an intermediate phenotype, while mutation of residues at the edges of the IE1 CTD had no

545 significant negative (G476, G477, K478, A489, and Q491) or even positive (D490) effects on
546 chromosome association (Fig. 4A–B).

547 These results identify a ten-amino-acid nucleosome binding motif (NBM: STHPMVTRSK)
548 within the IE1 CTD, of which amino acids H481, M483, T485, and R486 are individually
549 essential for nucleosome core targeting and chromosome attachment (Fig. 4D).

550

551 **Histone binding by the IE1 CTD is directed by acidic residues in H2A.** In addition to
552 identifying the viral determinants of IE1-nucleosome complex formation, we set out to probe the
553 histone-specific contributions. Much of the LANA-nucleosome interaction is mediated by
554 negatively charged residues in H2A composing the acidic pocket (12). Given the similarities in
555 histone binding between the LANA and IE1 CTDs (see Fig. 2), each of the nine negatively
556 charged amino acids found in H2A (including acidic pocket residues E56, E61, E64, D90, E91,
557 and E92) (Fig. 5A) was individually replaced with alanine. Additionally, we constructed two
558 triple mutants where H2A residues E61, E64, and D90 or D90, E91, and E92 were
559 simultaneously changed to alanine. Subsequently, human cells were transfected with plasmids
560 encoding epitope-tagged wild-type or mutant H2A, and pull-down assays with acid-extracted
561 histones and GST-IE1$_{476\text{-}491}$ were conducted (Fig. 5B). Interestingly, only mutations in acidic
562 pocket residues E56, E61, E64, and D90 and the two triple substitutions proved to abolish IE1-
563 H2A binding while all other mutations (E41A, D72A, E91A, E92A, and E121A) had little, if any,
564 effect on this interaction.

565 To confirm these results in the context of the full-length IE1 protein, we performed
566 additional immunoprecipitation-immunoblotting assays (Fig. 5C–D). Again, the E41A, D72A,
567 E91A, E92A, and E121A substitutions did not diminish (but rather enhanced) IE1 binding
568 relative to wild-type H2A. However, we reproducibly found reduced binding between the viral

569 protein and H2A mutants E56A, E61A, E64A, D90A, and D90A/E91A/E92A. In addition, the
570 E61A/E64A/D90A mutant exhibited highly impaired IE1 binding. As expected, neither of the
571 histone mutants was completely defective for binding to the viral protein, most likely due to the
572 second histone binding domain located upstream of the CTD (see Fig. 2B–C). Correspondingly,
573 $IE1_{1\text{-}475}$ retained some affinity for H2A (Fig. 5C–D).

574 These results demonstrate that several negatively charged H2A residues (E56, E61, E64,
575 and D90) composing the nucleosomal acidic pocket, but not acidic residues outside the pocket,
576 selectively direct the interaction with the IE1 CTD.

577

578 **The IE1 and LANA CTDs compete for binding to nucleosome cores and**
579 **chromosomes.** Our results indicate that IE1 targets human chromatin via interaction between its
580 CTD and the acidic pocket formed by H2A-H2B on nucleosome cores (see Fig. 2–5), which
581 closely resembles the situation described for LANA (12). To further test the idea that the IE1 and
582 LANA CTDs target the same nucleosomal surface, we asked whether the presence of the IE1
583 CTD is compatible with or competitive to nucleosome binding by the LANA CTD. First, we
584 utilized a competition pull-down assay to address this question. GST-$LANA_{5\text{-}22}$ was reacted with
585 acid-extracted histone octamers and increasing molar ratios of purified IE1. As observed
586 beforehand for IE1 (see Fig. 3B), histone binding by LANA extended to all four core histone
587 species under these conditions. However, IE1 diminished complex formation between the LANA
588 CTD and core histones in a dose-dependent manner (Fig. 6A). Compared to full-length IE1, the
589 CTD-deficient protein ($IE1_{1\text{-}475}$) was much less efficient in competing with GST-$LANA_{5\text{-}22}$ for
590 histone binding (Fig. 6B). Very similar results were obtained when a synthetic peptide
591 encompassing the LANA CTD (LANA-CTD) was used to compete with binding between GST-
592 $IE1_{476\text{-}491}$ and core histones, while a mutant peptide (LANA-CTD*) had no effect (Fig. 6C).

593 To gain *in vivo* support for our assumption that the IE1 and LANA CTDs compete for
594 binding to nucleosomes, we expressed HA-tagged IE1 and $LANA_{5-22}$ fused to EGFP in human
595 cells and examined their localization by immunofluorescence microscopy. In mitotic cells, both
596 EGFP-$LANA_{5-22}$ and HA-IE1 predominantly localized to condensed chromatin when expressed
597 individually (with HA or EGFP, respectively) conforming to previous observations (e.g., 12, 20,
598 22, 24, 59). However, simultaneous expression of the two proteins resulted in partial release of
599 EGFP-$LANA_{5-22}$ and almost complete displacement of HA-IE1 from mitotic chromatin. As
600 expected, HA-IE1 lacking the CTD (HA-$IE1_{1-475}$) did not attach to chromosomes (Fig. S3). These
601 results strongly suggest that IE1 and LANA share the same binding site on the nucleosome.
602
603 **The IE1 CTD is predicted to form a β-hairpin recognizing the acidic pocket on the**
604 **nucleosomal surface.** The notion of a shared binding site for IE1 and LANA on the nucleosome
605 also suggests that key residues responsible for CTD-histone interaction may be conserved
606 between the two viral proteins. Therefore, we generated alignments between the IE1 and LANA
607 CTD sequences. The algorithm implemented in PERMOL (54, 62) and most other tested
608 programs (e. g., ClustalW2, European Bioinformatics Institute) produced an alignment with three
609 identical residues, one conserved exchange, and two semi-conserved substitutions between
610 $LANA_{4-17}$ and $IE1_{476-491}$ (Fig. 7A). However, the same number of identical residues was also
611 found with an alternative alignment (Fig. S4A) generated by another program (LALIGN,
612 European Bioinformatics Institute). The two alignments differ mainly in the way the RS sequence
613 (R486–S487) in the IE1 CTD is positioned relative to either of two RS sequences (R9–S10 and
614 R12–S13) in the LANA CTD. Other possible alignments were excluded as they did not involve
615 the LANA residues known to be required for nucleosome binding (12).

Based on the two most likely alignments and the available x-ray structure of the LANA amino-terminal peptide bound to the nucleosome core (Protein Data Bank [PDB]: 1zla), molecular dynamics-based homology modeling of the IE1 CTD-histone complex was performed. From the patterns of hydrogen bonds, interatomic distances, and dihedral angles (54, 62) two sets of restraints (one for each alignment) were created and used to calculate 1,000 structures by restrained simulated annealing. The ten best structures each in terms of lowest total energy were refined in explicit water resulting in structural bundles (Fig. 7B and Fig. S4B). The results suggest that the IE1 CTD can adopt a β-hairpin (two antiparallel β-strands connected by a reverse turn) resembling the LANA CTD structure. The structural bundle deduced from the first of the two alignments is well defined with a backbone root-mean-square deviation (RMSD) of 0.038 nm (Fig. 7B). In this model, the β-hairpin formed by the IE1 CTD is stabilized by four main chain intramolecular hydrogen bonds, and there are ten intermolecular hydrogen bonds between CTD residues and histones H2A-H2B including amino acids forming the acidic pocket (Fig. 7C). A three-dimensional representation of this model indicates excellent shape and charge complementarity between the IE1 CTD and the acidic pocket formed by H2A-H2B including H2A residues E56, E61, E64, and E92 (Fig. 7D–E and Movie S1). The model derived from the second alignment is structurally much less well defined exhibiting a backbone RMSD of 0.200 nm (Fig. S4B). Here, the CTD engages in only three intra- and five intermolecular hydrogen bonds (Fig. S4C).

Although both interaction models largely comply with our *in vitro* and *in vivo* data, the *in silico* results and conclusions from mutagenesis experiments (see Discussion) favor the model shown in Fig. 7.

The IE1 CTD is dispensable for productive replication of "clinical" hCMV strains. To address how IE1-nucleosome interaction may impact the course and outcome of infection, BAC clones of the hCMV low passage strains TB40E (TBwt) and FIX (FXwt) were used to construct mutant viruses specifically lacking the IE1 CTD (TBIE1$_{1\text{-}475}$ and FXIE1$_{1\text{-}475}$, respectively). We also generated "revertant" viruses (TBrvIE1$_{1\text{-}475}$ and FXrvIE1) to control for inadvertent genetic changes. The IE1$_{1\text{-}475}$ proteins expressed from the mutant genomes were detected at kinetics and steady-state levels comparable to full-length IE1 (Fig. 8A–B), and the mutant proteins were confirmed to be inactive for chromosome association (Fig. 8C–D) in hCMV-infected cells.

Following infection of permissive fibroblast cells (MRC-5), two independent clones each of TBIE1$_{1\text{-}475}$ and FXIE1$_{1\text{-}475}$ did not exhibit significantly altered replication compared to the corresponding wild-type and revertant strains, neither at high nor low input multiplicities, as determined by quantification of extracellular viral DNA and infectious particles (Fig. 9). These findings are consistent with results from a recent study testing a CTD-deleted mutant of the hCMV high passage strain Towne (23). Thus, nucleosome targeting by IE1 appears to be entirely dispensable for normal productive hCMV infection in fibroblasts suggesting a function during non-productive infection and/or infection of other cell types (see Discussion).

DISCUSSION

Structural aspects of the IE1-nucleosome interaction. Nucleosomes are the repeating centerpieces of chromatin (reviewed in 3, 4). Within the nucleosome core, the disordered histone tail domains are known to engage in interactions with numerous different proteins, while the folded regions are believed to primarily function in compacting and constraining the DNA. However, the nucleosome surface is highly contoured and differentially charged (1, 2). The most distinctive feature of this surface is the acidic pocket, a negatively charged and concave patch generated by several highly conserved glutamate and aspartate residues contributed by histone H2A and, to a lesser extent, H2B (reviewed in 63, 64). In fact, the acidic pocket is the only negatively charged area on the otherwise positive or hydrophobic nucleosomal surface. The pocket serves no apparent role in maintaining the structure of the nucleosome, but is specifically recognized by histone H4 tails of adjacent nucleosomes (1, 2) and an increasing number of non-histone cellular and viral proteins. The first protein, besides histone H4, reported to bind to the acidic pocket was LANA encoded by the γ-herpesvirus KSHV (12). Subsequently, human interleukin 33 (IL-33) (61), *Drosophila melanogaster* regulator of chromosome condensation 1 (RCC1) (65), human high-mobility group nucleosomal 2 (HMGN2) protein (66), and *Saccharomyces cerevisiae* silent information regulator 3 (Sir3) (67) were all shown or predicted to interact with the acidic pocket of the nucleosomal core. Furthermore, Foamy virus group-specific antigen (Gag) and Borna disease virus ribonucleoprotein (RNP) were proposed to bind to host chromosomes via H2A-H2B (68, 69).

The present study identifies the first β-herpesvirus protein targeting the acidic pocket on the nucleosome. Previous work has demonstrated that the hCMV IE1 protein attaches to human

678 mitotic chromosomes through a CTD located at the carboxy-terminus (20, 22, 24). However, the
679 mechanism of interaction has not been addressed. Although hCMV encodes several chromatin-
680 associated proteins (e.g., 70, 71; reviewed in 72-76), nucleosome binding appears to be a rather
681 unique feature of IE1. For instance, the hCMV IE2 protein is known to interact with DNA (e.g.,
682 77-80), histones H3-H4 (81), and several histone-associated proteins (e.g., 51, 81-83); however,
683 IE2 neither associates with condensed chromatin (21, 25) nor with nucleosomes (this work), at
684 least not to the same extent as IE1. Surprisingly, even mIE1 has little affinity for nucleosomes
685 and does not co-localize with mitotic chromatin (21, 84 and this work) despite reportedly binding
686 to DNA and core histones (85, 86). Accordingly, IE1 orthologs of known rodent CMVs
687 (including mCMV and rat CMV strains) do not seem to exhibit functional CTD sequences (data
688 not shown). However, CTD and NBM sequences are highly conserved across IE1 proteins of
689 primate CMVs (Fig. 10) (22). The African green monkey CMV IE1 ortholog has also been
690 shown to associate with metaphase chromosomes (29). At the same time, sequence similarity
691 across the full-length orthologous IE1 proteins is limited (Fig. 10). Thus, any available evidence
692 points to nucleosome targeting being a primate-specific viral adaptation and a distinguishing
693 feature of primate CMV IE1 proteins.

694 Our results indicate that the IE1 NBM directly and selectively recognizes the nucleosome
695 core through the H2A-H2B dimer. In fact, IE1 does not detectably interact with linker histone
696 H1, and nucleic acids are not required for nucleosome binding by the viral protein. The latter
697 finding matches the long-standing assumption that hCMV IE1 does not directly bind to DNA
698 (86), although our data do not exclude this possibility. Despite the fact that the CTD is sufficient
699 for H2A-H2B binding, nucleosome core interaction, and chromosome association, histone
700 binding by IE1 is clearly not restricted to the carboxy-terminal domain. Instead, another histone
701 binding region, which functions independently from the CTD/NBM, must exist upstream of

amino acid 476. In contrast to the NBM, this region directly binds to all four core histones with a preference for H3-H4. The fact that all tested H2A mutants retain some affinity for full-length IE1 suggests that the upstream histone binding domain may interact with H2A-H2B residues outside the acidic patch. It is tempting to speculate that negatively charged residues within three proximate acidic stretches (termed acidic domains 1 to 3, AD1–AD3) (21) between amino acids 373 and 475 of IE1 might engage in electrostatic interactions with basic residues of the H3-H4 tetramer and the H2A-H2B dimers. Moreover, the observation that $IE1_{1\text{-}475}$ does not associate with chromosomes and is not required for nucleosome interaction suggests that the upstream histone binding region may interact with "free" histones rather than nucleosomes.

In most published cases of interactions with the nucleosomal acidic pocket (H4, LANA, IL-33, RCC1, and HMGN2), arginine (and serine) containing linear motifs within conformationally flexible protein regions contribute to H2A binding. Our work identifies the ten-amino-acid sequence STHPMVTRSK to be this motif in IE1 (NBM). Results from proton nuclear magnetic resonance spectroscopy suggest that the IE1 CTD is highly mobile and that this domain is natively unstructured (data not shown), as has been previously predicted (21). Nonetheless, our results strongly suggest that the IE1 CTD forms a loop connecting two hydrogen-bonded antiparallel β-sheets (β-hairpin), at least when complexed with H2A-H2B ("induced fit"). The predicted IE1 β-hairpin closely resembles the structure previously reported for the complexed LANA CTD (12). Consequently, the mode of interaction with nucleosomes is strikingly similar for IE1 and LANA; this is not only evident from our binding and competition experiments, but also from comparisons between our preferred model and the known crystal structure of the IE1 and LANA CTD-nucleosome complexes, respectively. According to the published structure (12), $LANA_{4\text{-}17}$ interacts with E61, E64, D90, and E92 of H2A (and several residues of H2B).

725 Likewise, our preferred model displays interactions between $IE1_{476-491}$ and H2A E61, E64, and
726 E92 (and H2B). In addition, substitution of H2A D90 has a strongly adverse effect on IE1
727 binding that cannot be directly inferred from the proposed hydrogen bond patterns. However, the
728 imidazole ring of IE1 H481 is expected to be positively charged in the complex and may thus be
729 involved in an electrostatic interaction with the nearby negatively charged side chain of H2A
730 D90. Most likely, the D90A exchange also alters the geometry of the IE1 H481 binding site
731 within the acidic pocket. Interestingly, our model predicts an additional interaction of $IE1_{476-491}$
732 with H2A E56 which has not been described for LANA. The importance of E56 for the IE1-
733 nucleosome interaction is reinforced by our mutational analyses. Moreover, the fact that E56 is
734 not predicted to contribute to H2A-IE1 binding by our alternative model adds further
735 experimental support in favor of the preferred model. Taken together, our structural data indicate
736 that LANA and IE1 target nucleosomes through molecular interactions that are highly similar,
737 albeit not identical.
738
739 **Potential functions of the IE1-nucleosome interaction.** Our structural analyses strongly
740 suggest that the IE1 CTD has specifically evolved to fit the acidic pocket of the nucleosome, and
741 the CTD/NBM sequences are highly and selectively conserved through primate CMV evolution.
742 These findings clearly point to an important role of nucleosome targeting by IE1 in hCMV
743 infection. However, no such role has been reported so far.
744 Our prior work has demonstrated that nucleosomes are not confined to cellular chromatin,
745 but also form on hCMV nuclear DNA (87-89). We have also recently shown that global
746 nucleosome occupancy and dynamics across hCMV genomes are largely controlled by IE1-
747 dependent mechanisms (88). Thus, IE1 may target nucleosomes for active remodeling of viral
748 and/or cellular chromatin. Notably, interaction between the acidic pocket contributed by H2A-

749 H2B and a positively charged region of the histone H4 tail from an adjacent nucleosome has been
750 implicated in the formation of higher-order chromatin structures (90, 91). The H4 tail has no
751 significant sequence similarity with the IE1 or LANA CTDs (data not shown) and seems to adopt
752 a different conformation compared to the viral peptides. Moreover, the binding sites of LANA
753 (and hence also of IE1) and H4 in the acidic pocket do not overlap (2, 12). Nonetheless, the
754 available structures and models predict that IE1 and LANA may displace the H4 tail from the
755 pocket raising the possibility that the viral proteins might adversely affect chromatin
756 condensation. Conceivably, global chromatin decondensation may serve as a mechanism through
757 which viruses enhance permissiveness of the cellular and/or viral genome to transcriptional
758 activation and/or other DNA-based processes. Luger and colleagues have examined the effect of
759 LANA CTD binding on folding and self-association of nucleosome arrays. Against expectations,
760 they found that LANA stabilizes self-association of nucleosomes and promotes cellular
761 heterochromatin formation (92). However, these findings somewhat conflict with other reports
762 (e.g., 93). Likewise, IL-33 appears to regulate chromatin compaction by promoting nucleosome-
763 nucleosome interactions (61). It remains to be determined whether IE1 has any positive or
764 negative effects on higher-order chromatin structure.

765 The CTD has been shown to be entirely dispensable for complementing the defective
766 replication of an IE1-deficient mutant hCMV (Towne) in human fibroblasts (22). Moreover,
767 mutant viruses of both laboratory-adapted and "clinical" hCMV strains expressing $IE1_{1-475}$
768 instead of the full-length protein do not display any obvious phenotypic differences compared to
769 the parental wild-type viruses in these cells (23 and this work). Thus, nucleosome binding by IE1
770 appears to be irrelevant for hCMV productive infection in fibroblasts. However, IE1-nucleosome
771 interaction may serve an important function in cell types supporting non-productive (latent)
772 hCMV infections. More than a decade ago, it was first reported that LANA tethers KSHV

episomes to host mitotic chromosomes (13, 94), and LANA turned out to be necessary and sufficient for KSHV episome persistence in the absence of other viral genes. By bridging KSHV DNA and host chromosomes, LANA facilitates nuclear retention and segregation of viral episomes to daughter nuclei during viral latency (reviewed in 95). Very similar mechanisms are used by EBNA1 of EBV and the early 2 (E2) proteins of human and bovine papillomaviruses, which also tether their respective genomes to cellular chromosomes for efficient maintenance during cell division (reviewed in 96). As opposed to other DNA viruses, including both α- and γ-herpesviruses, the mechanism of viral genome persistence during latency has remained a mystery in any of the β-herpesviruses. Thus it is highly tempting to speculate that the IE1-nucleosome interaction described in this work may contribute to hCMV genome tethering and maintenance.

ACKNOWLEDGMENTS

We would like to thank Robert Eisenman (Seattle, USA), Roger Everett (Glasgow, UK), Ronald Hay (Dundee, UK), Christian Sinzger (Ulm, Germany), Karsten Tischer (Berlin, Germany), and Dong Yu (St. Louis, USA) for important reagents, Ines Tschertner (Regensburg, Germany) for expert technical assistance, and Aloys Schepers (Munich, Germany) and Einat Zalckvar (Rehovot, Israel) for helpful comments.

This work was supported by grants from the Deutsche Forschungsgemeinschaft (NE791/2-2), the Human Frontier Science Program (RGY0071/2008), the Bayerische Forschungsstiftung, and by intramural funds from the Institute for Medical Microbiology and Hygiene.

REFERENCES

1. **Davey CA, Sargent DF, Luger K, Mäder AW, Richmond TJ.** 2002. Solvent mediated interactions in the structure of the nucleosome core particle at 1.9 Å resolution. J. Mol. Biol. **319:**1097-1113.
2. **Luger K, Mäder AW, Richmond RK, Sargent DF, Richmond TJ.** 1997. Crystal structure of the nucleosome core particle at 2.8 Å resolution. Nature **389:**251-260.
3. **Luger K, Dechassa ML, Tremethick DJ.** 2012. New insights into nucleosome and chromatin structure: an ordered state or a disordered affair? Nat. Rev. Mol. Cell Biol. **13:**436-447.
4. **Andrews AJ, Luger K.** 2011. Nucleosome structure(s) and stability: variations on a theme. Annu. Rev. Biophys. **40:**99-117.
5. **Sears J, Ujihara M, Wong S, Ott C, Middeldorp J, Aiyar A.** 2004. The amino terminus of Epstein-Barr Virus (EBV) nuclear antigen 1 contains AT hooks that facilitate the replication and partitioning of latent EBV genomes by tethering them to cellular chromosomes. J. Virol. **78:**11487-11505.
6. **Kapoor P, Frappier L.** 2003. EBNA1 partitions Epstein-Barr virus plasmids in yeast cells by attaching to human EBNA1-binding protein 2 on mitotic chromosomes. J. Virol. **77:**6946-6956.
7. **Kapoor P, Shire K, Frappier L.** 2001. Reconstitution of Epstein-Barr virus-based plasmid partitioning in budding yeast. EMBO J. **20:**222-230.

814 8. **Shire K, Ceccarelli DF, Avolio-Hunter TM, Frappier L.** 1999. EBP2, a human protein
815 that interacts with sequences of the Epstein-Barr virus nuclear antigen 1 important for
816 plasmid maintenance. J. Virol. **73:**2587-2595.
817 9. **Wu H, Ceccarelli DF, Frappier L.** 2000. The DNA segregation mechanism of Epstein-
818 Barr virus nuclear antigen 1. EMBO Rep. **1:**140-144.
819 10. **Krithivas A, Fujimuro M, Weidner M, Young DB, Hayward SD.** 2002. Protein
820 interactions targeting the latency-associated nuclear antigen of Kaposi's sarcoma-associated
821 herpesvirus to cell chromosomes. J. Virol. **76:**11596-11604.
822 11. **Barbera AJ, Chodaparambil JV, Kelley-Clarke B, Luger K, Kaye KM.** 2006. Kaposi's
823 sarcoma-associated herpesvirus LANA hitches a ride on the chromosome. Cell Cycle
824 **5:**1048-1052.
825 12. **Barbera AJ, Chodaparambil JV, Kelley-Clarke B, Joukov V, Walter JC, Luger K,**
826 **Kaye KM.** 2006. The nucleosomal surface as a docking station for Kaposi's sarcoma
827 herpesvirus LANA. Science **311:**856-861.
828 13. **Cotter MA, 2nd, Robertson ES.** 1999. The latency-associated nuclear antigen tethers the
829 Kaposi's sarcoma-associated herpesvirus genome to host chromosomes in body cavity-
830 based lymphoma cells. Virology **264:**254-264.
831 14. **Paulus C, Nevels M.** 2009. The human cytomegalovirus major immediate-early proteins as
832 antagonists of intrinsic and innate antiviral host reponses. Viruses **1:**760-779.
833 15. **Meier JL, Stinski MF.** 2013. Major immediate-early enhancer and its gene products, p
834 152–173. *In* Reddehase MJ (ed), Cytomegaloviruses: from molecular pathogenesis to
835 intervention, 2nd ed, vol 1. Caister Academic Press, Norfolk, United Kingdom.

16. **Mocarski ES, Shenk T, Pass RF.** 2007. Cytomegaloviruses, p 2701–2772. *In* Knipe DM, Howley PM (ed), Fields virology, 5th ed, vol 2. Lippincott Williams & Wilkins, Philadelphia, PA.

17. **Mocarski ES, Kemble GW, Lyle JM, Greaves RF.** 1996. A deletion mutant in the human cytomegalovirus gene encoding IE1(491aa) is replication defective due to a failure in autoregulation. Proc. Natl. Acad. Sci. U. S. A. **93:**11321-11326.

18. **Greaves RF, Mocarski ES.** 1998. Defective growth correlates with reduced accumulation of a viral DNA replication protein after low-multiplicity infection by a human cytomegalovirus ie1 mutant. J. Virol. **72:**366-379.

19. **Gawn JM, Greaves RF.** 2002. Absence of IE1 p72 protein function during low-multiplicity infection by human cytomegalovirus results in a broad block to viral delayed-early gene expression. J. Virol. **76:**4441-4455.

20. **Lafemina RL, Pizzorno MC, Mosca JD, Hayward GS.** 1989. Expression of the acidic nuclear immediate-early protein (IE1) of human cytomegalovirus in stable cell lines and its preferential association with metaphase chromosomes. Virology **172:**584-600.

21. **Krauss S, Kaps J, Czech N, Paulus C, Nevels M.** 2009. Physical requirements and functional consequences of complex formation between the cytomegalovirus IE1 protein and human STAT2. J. Virol. **83:**12854-12870.

22. **Reinhardt J, Smith GB, Himmelheber CT, Azizkhan-Clifford J, Mocarski ES.** 2005. The carboxyl-terminal region of human cytomegalovirus IE1491aa contains an acidic domain that plays a regulatory role and a chromatin-tethering domain that is dispensable during viral replication. J. Virol. **79:**225-233.

23. **Shin HJ, Kim YE, Kim ET, Ahn JH.** 2012. The chromatin-tethering domain of human cytomegalovirus immediate-early (IE) 1 mediates associations of IE1, PML and STAT2

with mitotic chromosomes, but is not essential for viral replication. J. Gen. Virol. **93:**716-721.

24. **Wilkinson GW, Kelly C, Sinclair JH, Rickards C.** 1998. Disruption of PML-associated nuclear bodies mediated by the human cytomegalovirus major immediate early gene product. J. Gen. Virol. **79:**1233-1245.

25. **Dimitropoulou P, Caswell R, McSharry BP, Greaves RF, Spandidos DA, Wilkinson GW, Sourvinos G.** 2010. Differential relocation and stability of PML-body components during productive human cytomegalovirus infection: Detailed characterization by live-cell imaging. Eur. J. Cell Biol. **89:**757-768.

26. **Ahn JH, Brignole EJ, 3rd, Hayward GS.** 1998. Disruption of PML subnuclear domains by the acidic IE1 protein of human cytomegalovirus is mediated through interaction with PML and may modulate a RING finger-dependent cryptic transactivator function of PML. Mol. Cell. Biol. **18:**4899-4913.

27. **Huh YH, Kim YE, Kim ET, Park JJ, Song MJ, Zhu H, Hayward GS, Ahn JH.** 2008. Binding STAT2 by the acidic domain of human cytomegalovirus IE1 promotes viral growth and is negatively regulated by SUMO. J. Virol. **82:**10444-10454.

28. **Nevels M, Brune W, Shenk T.** 2003. SUMOylation of the human cytomegalovirus major immediate-early protein IE1-72kDa contributes to efficient viral replication by promoting the accumulation of IE2-86kDa. J. Virol. **78:**7803-7812.

29. **Chang YN, Jeang KT, Lietman T, Hayward GS.** 1995. Structural organization of the spliced immediate-early gene complex that encodes the major acidic nuclear (IE1) and transactivator (IE2) proteins of African green monkey cytomegalovirus. J. Biomed. Sci. **2:**105-130.

30. **Tanaka M, Herr W.** 1990. Differential transcriptional activation by Oct-1 and Oct-2: interdependent activation domains induce Oct-2 phosphorylation. Cell **60:**375-386.

31. **Maruyama K, Takebe Y.** 1990. New trend of cDNA cloning. Med. Immunol. (Tokyo) **20:**27-32.

32. **Guan KL, Dixon JE.** 1991. Eukaryotic proteins expressed in Escherichia coli: an improved thrombin cleavage and purification procedure of fusion proteins with glutathione S-transferase. Anal. Biochem. **192:**262-267.

33. **Tatham MH, Jaffray E, Vaughan OA, Desterro JM, Botting CH, Naismith JH, Hay RT.** 2001. Polymeric chains of SUMO-2 and SUMO-3 are conjugated to protein substrates by SAE1/SAE2 and Ubc9. J. Biol. Chem. **276:**35368-35374.

34. **Baldick CJ, Jr., Marchini A, Patterson CE, Shenk T.** 1997. Human cytomegalovirus tegument protein pp71 (ppUL82) enhances the infectivity of viral DNA and accelerates the infectious cycle. J. Virol. **71:**4400-4408.

35. **Shiio Y, Eisenman RN.** 2003. Histone sumoylation is associated with transcriptional repression. Proc. Natl. Acad. Sci. U. S. A. **100:**13225-13230.

36. **Ho SN, Hunt HD, Horton RM, Pullen JK, Pease LR.** 1989. Site-directed mutagenesis by overlap extension using the polymerase chain reaction. Gene **77:**51-59.

37. **Jacobs JP, Jones CM, Baille JP.** 1970. Characteristics of a human diploid cell designated MRC-5. Nature **227:**168-170.

38. **Mitsudomi T, Steinberg SM, Nau MM, Carbone D, D'Amico D, Bodner S, Oie HK, Linnoila RI, Mulshine JL, Minna JD, et al.** 1992. p53 gene mutations in non-small-cell lung cancer cell lines and their correlation with the presence of ras mutations and clinical features. Oncogene **7:**171-180.

906 39. **Plotkin SA, Furukawa T, Zygraich N, Huygelen C.** 1975. Candidate cytomegalovirus
907 strain for human vaccination. Infect. Immun. **12:**521-527.
908 40. **Knoblach T, Grandel B, Seiler J, Nevels M, Paulus C.** 2011. Human cytomegalovirus
909 IE1 protein elicits a type II interferon-like host cell response that depends on activated
910 STAT1 but not interferon-γ. PLoS Pathog **7:**e1002016.
911 41. **Marchini A, Liu H, Zhu H.** 2001. Human cytomegalovirus with IE-2 (UL122) deleted
912 fails to express early lytic genes. J. Virol. **75:**1870-1878.
913 42. **Riegler S, Hebart H, Einsele H, Brossart P, Jahn G, Sinzger C.** 2000. Monocyte-derived
914 dendritic cells are permissive to the complete replicative cycle of human cytomegalovirus.
915 J. Gen. Virol. **81:**393-399.
916 43. **Sinzger C, Hahn G, Digel M, Katona R, Sampaio KL, Messerle M, Hengel H,**
917 **Koszinowski U, Brune W, Adler B.** 2008. Cloning and sequencing of a highly productive,
918 endotheliotropic virus strain derived from human cytomegalovirus TB40/E. J. Gen. Virol.
919 **89:**359-368.
920 44. **Tischer BK, Smith GA, Osterrieder N.** 2010. En passant mutagenesis: a two step
921 markerless red recombination system. Methods Mol. Biol. **634:**421-430.
922 45. **Tischer BK, von Einem J, Kaufer B, Osterrieder N.** 2006. Two-step red-mediated
923 recombination for versatile high-efficiency markerless DNA manipulation in *Escherichia*
924 *coli.* Biotechniques **40:**191-197.
925 46. **Gerna G, Percivalle E, Sarasini A, Baldanti F, Revello MG.** 2002. The attenuated
926 Towne strain of human cytomegalovirus may revert to both endothelial cell tropism and
927 leuko- (neutrophil- and monocyte-) tropism in vitro. J. Gen. Virol. **83:**1993-2000.

47. **Hahn G, Khan H, Baldanti F, Koszinowski UH, Revello MG, Gerna G.** 2002. The human cytomegalovirus ribonucleotide reductase homolog UL45 is dispensable for growth in endothelial cells, as determined by a BAC-cloned clinical isolate of human cytomegalovirus with preserved wild-type characteristics. J. Virol. **76:**9551-9555.

48. **Smith GA, Enquist LW.** 1999. Construction and transposon mutagenesis in Escherichia coli of a full-length infectious clone of pseudorabies virus, an alphaherpesvirus. J. Virol. **73:**6405-6414.

49. **Yu D, Smith GA, Enquist LW, Shenk T.** 2002. Construction of a self-excisable bacterial artificial chromosome containing the human cytomegalovirus genome and mutagenesis of the diploid TRL/IRL13 gene. J. Virol. **76:**2316-2328.

50. **Rodriguez-Collazo P, Leuba SH, Zlatanova J.** 2009. Robust methods for purification of histones from cultured mammalian cells with the preservation of their native modifications. Nucleic Acids Res. **37:**e81.

51. **Nevels M, Paulus C, Shenk T.** 2004. Human cytomegalovirus immediate-early 1 protein facilitates viral replication by antagonizing histone deacetylation. Proc. Natl. Acad. Sci. U. S. A. **101:**17234-17239.

52. **Zhu H, Shen Y, Shenk T.** 1995. Human cytomegalovirus IE1 and IE2 proteins block apoptosis. J. Virol. **69:**7960-7970.

53. **Graham FL, van der Eb AJ.** 1973. A new technique for the assay of infectivity of human adenovirus 5 DNA. Virology **52:**456-467.

54. **Möglich A, Weinfurtner D, Gronwald W, Maurer T, Kalbitzer HR.** 2005. PERMOL: restraint-based protein homology modeling using DYANA or CNS. Bioinformatics **21:**2110-2111.

55. **Gronwald W, Brunner K, Kirchhöfer R, Nasser A, Trenner J, Ganslmeier B, Riepl H, Ried A, Scheiber J, Elsner R, Neidig KP, Kalbitzer HR.** 2004. AUREMOL, a new program for the automated structure elucidation of biological macromolecules. Bruker Rep. **154/155:**11-14.

56. **Brunger AT.** 2007. Version 1.2 of the Crystallography and NMR system. Nat. Protoc. **2:**2728-2733.

57. **Brunger AT, Adams PD, Clore GM, DeLano WL, Gros P, Grosse-Kunstleve RW, Jiang JS, Kuszewski J, Nilges M, Pannu NS, Read RJ, Rice LM, Simonson T, Warren GL.** 1998. Crystallography & NMR system: A new software suite for macromolecular structure determination. Acta Crystallogr. D Biol. Crystallogr. **54:**905-921.

58. **Linge JP, Williams MA, Spronk CA, Bonvin AM, Nilges M.** 2003. Refinement of protein structures in explicit solvent. Proteins **50:**496-506.

59. **Piolot T, Tramier M, Coppey M, Nicolas JC, Marechal V.** 2001. Close but distinct regions of human herpesvirus 8 latency-associated nuclear antigen 1 are responsible for nuclear targeting and binding to human mitotic chromosomes. J. Virol. **75:**3948-3959.

60. **Shinohara H, Fukushi M, Higuchi M, Oie M, Hoshi O, Ushiki T, Hayashi J, Fujii M.** 2002. Chromosome binding site of latency-associated nuclear antigen of Kaposi's sarcoma-associated herpesvirus is essential for persistent episome maintenance and is functionally replaced by histone H1. J. Virol. **76:**12917-12924.

61. **Roussel L, Erard M, Cayrol C, Girard JP.** 2008. Molecular mimicry between IL-33 and KSHV for attachment to chromatin through the H2A-H2B acidic pocket. EMBO Rep. **9:**1006-1012.

62. **Möglich A, Weinfurtner D, Maurer T, Gronwald W, Kalbitzer HR.** 2005. A restraint molecular dynamics and simulated annealing approach for protein homology modeling utilizing mean angles. BMC Bioinformatics **6:**91.

63. **Kalashnikova AA, Porter-Goff ME, Muthurajan UM, Luger K, Hansen JC.** 2013. The role of the nucleosome acidic patch in modulating higher order chromatin structure. J. R. Soc. Interface **10:**20121022.

64. **Bönisch C, Hake SB.** 2012. Histone H2A variants in nucleosomes and chromatin: more or less stable? Nucleic Acids Res. **40:**10719-10741.

65. **Makde RD, England JR, Yennawar HP, Tan S.** 2010. Structure of RCC1 chromatin factor bound to the nucleosome core particle. Nature **467:**562-566.

66. **Kato H, van Ingen H, Zhou BR, Feng H, Bustin M, Kay LE, Bai Y.** 2011. Architecture of the high mobility group nucleosomal protein 2-nucleosome complex as revealed by methyl-based NMR. Proc. Natl. Acad. Sci. U. S. A. **108:**12283-12288.

67. **Armache KJ, Garlick JD, Canzio D, Narlikar GJ, Kingston RE.** 2011. Structural basis of silencing: Sir3 BAH domain in complex with a nucleosome at 3.0 Å resolution. Science **334:**977-982.

68. **Matsumoto Y, Hayashi Y, Omori H, Honda T, Daito T, Horie M, Ikuta K, Fujino K, Nakamura S, Schneider U, Chase G, Yoshimori T, Schwemmle M, Tomonaga K.** 2012. Bornavirus closely associates and segregates with host chromosomes to ensure persistent intranuclear infection. Cell Host Microbe **11:**492-503.

69. **Tobaly-Tapiero J, Bittoun P, Lehmann-Che J, Delelis O, Giron ML, de The H, Saib A.** 2008. Chromatin tethering of incoming foamy virus by the structural Gag protein. Traffic **9:**1717-1727.

70. **Terhune SS, Moorman NJ, Cristea IM, Savaryn JP, Cuevas-Bennett C, Rout MP, Chait BT, Shenk T.** 2010. Human cytomegalovirus UL29/28 protein interacts with components of the NuRD complex which promote accumulation of immediate-early RNA. PLoS Pathog. **6:**e1000965.

71. **Saffert RT, Kalejta RF.** 2006. Inactivating a cellular intrinsic immune defense mediated by Daxx is the mechanism through which the human cytomegalovirus pp71 protein stimulates viral immediate-early gene expression. J. Virol. **80:**3863-3871.

72. **Penkert RR, Kalejta RF.** 2011. Tegument protein control of latent herpesvirus establishment and animation. Herpesviridae **2:**3.

73. **Nevels M, Nitzsche A, Paulus C.** 2011. How to control an infectious bead string: nucleosome-based regulation and targeting of herpesvirus chromatin. Rev Med Virol. **21:**154-180.

74. **Paulus C, Nitzsche A, Nevels M.** 2010. Chromatinisation of herpesvirus genomes. Rev Med Virol **20:**34-50.

75. **Knipe DM, Lieberman PM, Jung JU, McBride AA, Morris KV, Ott M, Margolis D, Nieto A, Nevels M, Parks RJ, Kristie TM.** 2012. Snapshots: chromatin control of viral infection. Virology **435:**141-156.

76. **Reeves M, Sinclair J.** 2013. Regulation of human cytomegalovirus transcription in latency: beyond the major immediate-early promoter. Viruses **5:**1395-1413.

77. **Arlt H, Lang D, Gebert S, Stamminger T.** 1994. Identification of binding sites for the 86-kilodalton IE2 protein of human cytomegalovirus within an IE2-responsive viral early promoter. J. Virol. **68:**4117-4125.

78. **Macias MP, Stinski MF.** 1993. An in vitro system for human cytomegalovirus immediate early 2 protein (IE2)-mediated site-dependent repression of transcription and direct binding of IE2 to the major immediate early promoter. Proc. Natl. Acad. Sci. U. S. A. **90:**707-711.

79. **Waheed I, Chiou CJ, Ahn JH, Hayward GS.** 1998. Binding of the human cytomegalovirus 80-kDa immediate-early protein (IE2) to minor groove A/T-rich sequences bounded by CG dinucleotides is regulated by protein oligomerization and phosphorylation. Virology **252:**235-257.

80. **Ahn JH, Chiou CJ, Hayward GS.** 1998. Evaluation and mapping of the DNA binding and oligomerization domains of the IE2 regulatory protein of human cytomegalovirus using yeast one and two hybrid interaction assays. Gene **210:**25-36.

81. **Lee SB, Lee CF, Ou DS, Dulal K, Chang LH, Ma CH, Huang CF, Zhu H, Lin YS, Juan LJ.** 2011. Host-viral effects of chromatin assembly factor 1 interaction with HCMV IE2. Cell Res. **21:**1230-1247.

82. **Park JJ, Kim YE, Pham HT, Kim ET, Chung YH, Ahn JH.** 2007. Functional interaction of the human cytomegalovirus IE2 protein with histone deacetylase 2 in infected human fibroblasts. J. Gen. Virol. **88:**3214-3223.

83. **Reeves M, Murphy J, Greaves R, Fairley J, Brehm A, Sinclair J.** 2006. Autorepression of the human cytomegalovirus major immediate-early promoter/enhancer at late times of infection is mediated by the recruitment of chromatin remodeling enzymes by IE86. J. Virol. **80:**9998-10009.

84. **Maul GG, Negorev D.** 2008. Differences between mouse and human cytomegalovirus interactions with their respective hosts at immediate early times of the replication cycle. Med. Microbiol. Immunol. **197:**241-249.

85. **Münch K, Keil GM, Messerle M, Koszinowski UH.** 1988. Interaction of the 89K murine cytomegalovirus immediate-early protein with core histones. Virology **163:**405-412.

86. **Münch K, Messerle M, Plachter B, Koszinowski UH.** 1992. An acidic region of the 89K murine cytomegalovirus immediate early protein interacts with DNA. J. Gen. Virol. **73:**499-506.

87. **Nitzsche A, Paulus C, Nevels M.** 2008. Temporal dynamics of cytomegalovirus chromatin assembly in productively infected human cells. J. Virol. **82:**11167-11180.

88. **Zalckvar E, Paulus C, Tillo D, Asbach-Nitzsche A, Lubling Y, Winterling C, Strieder N, Mucke K, Goodrum F, Segal E, Nevels M.** 2013. Nucleosome maps of the human cytomegalovirus genome reveal a temporal switch in chromatin organization linked to a major IE protein. Proc. Natl. Acad. Sci. U. S. A. **110:**13126-13131.

89. **Nitzsche A, Steinhäußer C, Mücke K, Paulus C, Nevels M.** 2012. Histone H3 lysine 4 methylation marks postreplicative human cytomegalovirus chromatin. J. Virol. **6:**9817-9827.

90. **Dorigo B, Schalch T, Bystricky K, Richmond TJ.** 2003. Chromatin fiber folding: requirement for the histone H4 N-terminal tail. J. Mol. Biol. **327:**85-96.

91. **Kan PY, Caterino TL, Hayes JJ.** 2009. The H4 tail domain participates in intra- and internucleosome interactions with protein and DNA during folding and oligomerization of nucleosome arrays. Mol. Cell. Biol. **29:**538-546.

92. **Chodaparambil JV, Barbera AJ, Lu X, Kaye KM, Hansen JC, Luger K.** 2007. A charged and contoured surface on the nucleosome regulates chromatin compaction. Nat. Struct. Mol. Biol. **14:**1105-1107.

93. **Stuber G, Mattsson K, Flaberg E, Kati E, Markasz L, Sheldon JA, Klein G, Schulz TF, Szekely L.** 2007. HHV-8 encoded LANA-1 alters the higher organization of the cell nucleus. Mol. Cancer **6:**28.

94. **Ballestas ME, Chatis PA, Kaye KM.** 1999. Efficient persistence of extrachromosomal KSHV DNA mediated by latency-associated nuclear antigen. Science **284:**641-644.

95. **Ohsaki E, Ueda K.** 2012. Kaposi's sarcoma-associated herpesvirus genome replication, partitioning, and maintenance in latency. Front. Microbiol. **3:**1-12.

96. **Feeney KM, Parish JL.** 2009. Targeting mitotic chromosomes: a conserved mechanism to ensure viral genome persistence. Proc. Biol. Sci. **276:**1535-1544.

97. **DeLano WL.** 2002. The PyMOL user's manual. DeLano Scientific, San Carlos, CA.

98. **Benson DA, Karsch-Mizrachi I, Clark K, Lipman DJ, Ostell J, Sayers EW.** 2012. GenBank. Nucleic Acids Res. **40:**D48-53.

99. **Waterhouse AM, Procter JB, Martin DM, Clamp M, Barton GJ.** 2009. Jalview Version 2--a multiple sequence alignment editor and analysis workbench. Bioinformatics **25:**1189-1191.

100. **Crooks GE, Hon G, Chandonia JM, Brenner SE.** 2004. WebLogo: a sequence logo generator. Genome Res. **14:**1188-1190.

Figure Legends

FIG 1 hCMV IE1 interacts with human nucleosomes and all four core histones in a nucleic acid-independent fashion.

(A) Results of co-immunoprecipitations from plasmid-transfected cells. H1299 cells were transfected with plasmids encoding the indicated HA-tagged viral proteins or with empty vector (w/o). Cell extracts were combined with nucleosomes derived from MNase-digested human cell nuclei. Samples were subjected to immunoprecipitation using anti-HA or anti-Flag agarose. Input and output protein samples were separated in 10 or 15% polyacrylamide-SDS gels, and HA-tagged proteins and individual core histones were detected by immunoblotting. See also Fig. S1.

(B) Results of co-immunoprecipitations from hCMV-infected cells. Following infection of MRC-5 cells with TNwt or TNdlIE1 viruses (3 PFU/cell for 72 h), cells were fixed with formaldehyde, and cell extracts were sonicated to solubilize nucleosomes. Samples were subjected to immunoprecipitation using rabbit antibodies to histone H3 or non-specific rabbit IgG (rbIgG). Input and output protein samples were separated in 15% polyacrylamide-SDS gels, and the IE1 protein and histone H3 were detected by immunoblotting.

(C) Results of *in vitro* GST pull-down assays. Equal volumes of empty glutathione sepharose beads or beads carrying GST or GST-IE1 were reacted with acid-extracted human histones in the absence or presence of DNase I and RNase A. Input (8% of output) and output protein samples were separated in 15% polyacrylamide-SDS gels and stained with Coomassie Brilliant Blue.

FIG 2 hCMV IE1 exhibits two separable histone binding domains with differential specificities for H2A-H2B and H3-H4.

(A) Schematic of wild-type and mutant hCMV IE1 and KSHV LANA proteins with relative locations of their CTDs.

(B) Results of *in vitro* GST pull-down assays with acid-extracted unfractionated human histones. Empty glutathione sepharose beads or beads carrying GST or the indicated GST fusion proteins were reacted with acid-extracted human histones. Input and output protein samples were separated along with purified recombinant human core histones (H2A, H2B, H3, and H4 from New England Biolabs) in a 15% polyacrylamide-SDS gel and stained with Coomassie Brilliant Blue. The asterisk marks H1 histones.

(C) Results of *in vitro* GST pull-down assays with acid-extracted human histones separated into H2A-H2B and H3-H4 fractions. Equal volumes of empty glutathione sepharose beads or beads carrying GST or the indicated GST fusion proteins were reacted with purified human H2A-H2B or H3-H4. Input (8% of output) and output protein samples were separated in 15% polyacrylamide-SDS gels and stained with Coomassie Brilliant Blue.

FIG 3 Alanine scanning mutagenesis identifies IE1 CTD residues critical for histone binding.

(A) Presentation of wild-type (wt) and mutant $IE1_{476\text{-}491}$ protein sequences. Amino acids substituted by alanine scanning mutagenesis are highlighted.

(B) Results of *in vitro* GST pull-down assays. Glutathione sepharose beads carrying GST or the indicated wild-type (wt) and mutant GST-$IE1_{476\text{-}491}$ fusion proteins (see also Fig. 3A) were reacted with acid-extracted histones. Input (14% of output) and output protein samples were separated in 15% polyacrylamide-SDS gels and stained with Coomassie Brilliant Blue.

(C) Quantitative assessment of GST pull-down assay results. The output bands were quantified by densitometry, and bars represent the ratio of histones H3, H2B, H2A, and H4 to GST-$IE1_{476\text{-}}$

$_{491}$. Results for the CTD mutants are presented relative to the CTD wt sample present on the same gel (set to 100%).

FIG 4 Alanine scanning mutagenesis identifies IE1 CTD residues critical for mitotic chromatin association.

(A) Results of co-localization analyses in mitotic cells. H1299 cells were transfected with plasmids encoding EGFP or the indicated wild-type (wt) and mutant EGFP-IE1$_{476-491}$ fusion proteins (see also Fig. 3A). Cells were fixed with methanol, immunostained for EGFP, and counterstained for DNA with DAPI. Representative individual and merged images of EGFP and DAPI signals are presented.

(B) Quantitative assessment of co-localization analysis results. The extent of overlap between pixels in the green and blue channels was quantified by calculating Pearson's correlation coefficients (1 = perfect positive correlation, 0 = no correlation, -1 = perfect negative correlation). Bars represent means from at least three randomly selected mitotic cell images with standard deviations. A Student's t-test was performed to check for statistical significance of differences between CTD wt and the respective mutant (* p <0.1, ** p <0.01).

(C) Assessment of essential CTD residues in the background of full-length IE1. H1299 cells were transfected with pCMV.TetO-derived plasmids encoding wild-type IE1, IE1$_{1-475}$, or full-length IE1 with alanine substitutions of all four (IE1 NBM) or one single (IE1 M483A) CTD residue determined to be essential in (A) and (B). Cells were fixed with methanol, immunostained for IE1, and counterstained for DNA with DAPI. Representative individual and merged images of IE1 and DAPI signals are presented.

(D) Delineation of the nucleosome binding motif (NBM) within the IE1 CTD as deduced from data shown in (A), (B), (C), and Fig. 3. Amino acids determined to be essential or accessory for histone binding and chromatin association are highlighted.

FIG 5 Site-directed mutagenesis identifies human H2A residues critical for interaction with IE1.
(A) H2A residues targeted by mutagenesis and evaluated for contributions to IE1 binding. The complete sequence of human histone H2A.2 (H2A type 1-B/E) is shown, with acidic residues in bold letters and amino acids forming the acidic pocket underlined.
(B) Results of *in vitro* GST pull-down assays performed with the IE1 CTD. Empty glutathione sepharose beads or beads carrying GST-IE1$_{476-491}$ were reacted with acid-extracted human histones from H1299 cells transfected with empty vector (w/o) or plasmids encoding the indicated Flag-tagged H2A proteins. Input and output protein samples were separated in 15% polyacrylamide-SDS gels and stained with Coomassie Brilliant Blue. Flag-H2A proteins were detected by immunoblotting.
(C) Results of co-immunoprecipitations performed with full-length IE1 protein. H1299 cells were simultaneously transfected with empty vector (w/o) or plasmids encoding the indicated wild-type (wt) and mutant Flag-H2A proteins and plasmids encoding either HA-tagged full-length IE1 or HA-IE1$_{1-475}$. Cells were fixed with formaldehyde, and cell extracts were sonicated to solubilize nucleosomes. Samples were subjected to immunoprecipitation using anti-HA or mouse IgG (mIgG) agarose. Input and output protein samples were separated in 10 or 15% polyacrylamide-SDS gels, and Flag- and HA-tagged proteins were detected by immunoblotting.

(D) Quantitative assessment of results. The α-Flag bands shown in (C) were quantified by densitometry, and bars represent the ratio of output to input signal intensities relative to the H2A wt sample present on the same blot (set to 100%).

FIG 6 The IE1 and LANA CTDs compete for binding to human core histones.

(A) Full-length IE1 competes with GST-$LANA_{5-22}$ for histone binding.

(B) IE1 lacking the CTD ($IE1_{1-475}$) is less active in competing with GST-$LANA_{5-22}$ for histone binding compared to the full-length protein.

(C) A peptide encompassing $LANA_{5-22}$ (LANA-CTD), but not a mutant peptide (LANA-CTD*), interferes with histone binding to GST-$IE1_{476-491}$.

Acid-extracted human histones were combined with solvent or with the indicated soluble IE1 proteins (A, B) or LANA peptides (C) and then subjected to *in vitro* GST pull-down assays with glutathione sepharose beads carrying GST-$LANA_{5-22}$ (A, B) or GST-$IE1_{476-491}$ (C). Input and output protein samples were separated in 15% polyacrylamide-SDS gels and stained with Coomassie Brilliant Blue. See also Fig. S3.

FIG 7 The IE1 CTD is predicted to adopt a β-hairpin structure that docks with the acidic pocket formed by H2A-H2B on the nucleosomal surface.

(A) Amino acid sequence alignment of $IE1_{476-491}$ and $LANA_{4-17}$ (* = identical residue, : = conserved substitution, . = semi-conserved substitution) used for homology modeling.

(B) Bundles of the ten lowest total energy structures for $IE1_{476-491}$ after explicit water refinement (RMSD = 0.038 nm) based on the sequence alignment of (A) and the $LANA_{4-17}$-nucleosome crystal structure (PDB: 1zla).

(C) Predicted intra- and intermolecular hydrogen bonds in the $IE1_{476-491}$-nucleosome complex based on the sequence alignment of (A) and the $LANA_{4-17}$-nucleosome crystal structure (PDB: 1zla). Black arrows symbolize predicted interactions between IE1 CTD and H2A or H2B residues also observed in the LANA-nucleosome complex, and red arrows represent predicted interactions unique to the IE1-nucleosome complex. Arrow tails define the donor and arrow heads point at the acceptor of a possible hydrogen bond.

(D) Front view of detailed total best energy homology model of the molecular interaction between $IE1_{476-491}$ and the H2A-H2B dimer based on the sequence alignment of (A) and the $LANA_{4-17}$-nucleosome crystal structure after explicit water refinement. The model is presented as displayed in PyMOL (http://www.pymol.org) (97) showing the H2A-H2B dimer in surface representation. Blue color represents positively charged and red color negatively charged side chains. The H2A residues predicted or experimentally determined to be critical for binding to $IE1_{476-491}$ (see Fig. 5) are indicated. The $IE1_{476-491}$ peptide is shown in a ball-and-stick representation. IE1 residues P482 and R486 are marked by arrows for better orientation.

(E) Model (D) after 90° turn in indicated direction. See also Fig. S4 and Movie S1.

FIG 8 Steady-state levels and chromatin association of wild-type and mutant IE1 proteins in hCMV-infected cells.

(A) IE1 and IE2 steady-state protein levels in hCMV TB40E infections. MRC-5 cells were mock-infected or infected with TBwt, $TBrvIE1_{1-475}$, or $TBIE1_{1-475}$ at 3 PFU/cell, and viral IE1/IE2 protein levels were monitored over time by separation in 10% polyacrylamide-SDS gels and immunoblotting. Detection of the cellular GAPDH protein served as a loading control.

(B) IE1 and IE2 steady-state protein levels in hCMV FIX infections. MRC-5 cells were mock-infected or infected with FXwt, FXrvIE1, or $FXIE1_{1-475}$ at 3 PFU/cell, and viral IE1/IE2 protein

levels were monitored over time by separation in 10% polyacrylamide-SDS gels and immunoblotting. Detection of the cellular GAPDH protein served as a loading control.

(C) Mitotic chromatin association of IE1 in hCMV TB40E infections. MRC-5 cells were mock-infected or infected with TBwt, TBrvIE1$_{1-475}$, or TBIE1$_{1-475}$ at 3 PFU/cell for 48 h, and the localization of the viral IE1 protein relative to cellular mitotic chromatin (stained with DAPI) was detected by indirect immunofluorescence using a 1:1 mix of antibodies IE1.G10 and 6E1.

(D) Mitotic chromatin association of IE1 in hCMV FIX infections. MRC-5 cells were mock-infected or infected with FXwt, FXrvIE1, or FXIE1$_{1-475}$ at 3 PFU/cell for 48 h, and the localization of the viral IE1 protein relative to cellular mitotic chromatin (stained with DAPI) was detected by indirect immunofluorescence using antibody IE1.G10.

FIG 9 The IE1 CTD is not required for efficient hCMV productive infection.

(A) Single-step replication analysis of TB40E viruses. MRC-5 cells were infected with TBwt, TBrvIE1$_{1-475}$, or TBIE1$_{1-475}$ (two independent clones) at high input multiplicity (3 PFU/cell), and extracellular viral genomes were monitored over time by qPCR-based relative quantification. Data represent means and standard deviations from duplicate infections each measured twice (TBwt at 0 days post infection set to 1).

(B) Peak virus titers in high multiplicity TB40E infections. Extracellular infectious particles from 7 days post infection (A) were quantified by standard plaque assay on MRC-5 cells. Data represent means and standard deviations from duplicate infections each measured twice.

(C) Multi-step replication analysis of TB40E viruses. MRC-5 cells were infected with TBwt, TBrvIE1$_{1-475}$, or TBIE1$_{1-475}$ (two independent clones) at low input multiplicity (0.03 PFU/cell), and extracellular viral genomes were monitored over time by qPCR-based relative quantification.

Data represent means and standard deviations from duplicate infections each measured twice (TBwt at 0 days post infection set to 1).

(D) Peak virus titers in low multiplicity TB40E infections. Extracellular infectious particles from 16 days post infection (C) were quantified by standard plaque assay on MRC-5 cells. Data represent means and standard deviations from duplicate experiments each measured twice.

(E) Single-step replication analysis of FIX viruses. MRC-5 cells were infected with FXwt, FXrvIE1, or $FXIE1_{1\text{-}475}$ (two independent clones) at high input multiplicity (3 PFU/cell), and extracellular viral genomes were monitored over time by qPCR-based relative quantification. Data represent means and standard deviations from duplicate infections each measured twice (FXwt at 0 days post infection set to 1).

(F) Peak virus titers in high multiplicity FIX infections. Extracellular infectious particles from 6 days post infection (E) were quantified by standard plaque assay on MRC-5 cells. Data represent means and standard deviations from duplicate infections each measured twice.

(G) Multi-step replication analysis of FIX viruses. MRC-5 cells were infected with FXwt, FXrvIE1, or $FXIE1_{1\text{-}475}$ (two independent clones) at low input multiplicity (0.05 PFU/cell), and extracellular viral genomes were monitored over time by qPCR-based relative quantification. Data represent means and standard deviations from duplicate infections each measured twice (FXwt at 0 days post infection set to 1).

(H) Peak virus titers in low multiplicity FIX infections. Extracellular infectious particles from 15 days post infection (G) were quantified by standard plaque assay on MRC-5 cells. Data represent means and standard deviations from duplicate infections each measured twice.

FIG 10 The IE1 NBM is selectively conserved through primate CMV evolution.

(A) Alignment of orthologous IE1 sequences from hCMV (Towne) and all non-human primate CMV isolates present in GenBank (National Center for Biotechnology Information) (98) including chimpanzee CMV (panine herpesvirus 2), african green monkey (simian) CMV (cercopithecine herpesvirus 5), rhesus macaque CMV (*Macaca mulatta* CMV and Macacine herpesvirus 3, 68-1 strain), and baboon CMV. The multiple sequence alignment was generated using ClustalW2 (European Bioinformatics Institute; http://www.ebi.ac.uk/tools/msa/clustalw2) with default settings and rendered using Jalview 2.7 (http://www.jalview.org) (99). The extent of amino acid conservation is visualized by shades of blue. CTD and NBM sequences are marked.

(B) Table presenting GenBank accession numbers of orthologous IE1 sequences from primate CMVs and % amino acid sequence identities of full-length IE1 proteins, IE1 CTDs, and IE1 NBMs relative to the corresponding hCMV IE1 (Towne) sequence based on pairwise alignments (IE1) or the multiple sequence alignment shown in (A) (CTD, NBM).

(C) Sequence logo illustrating extent of amino acid conservation in orthologous IE1 CTD sequences from primate CMVs. The sequence logo was generated using WebLogo 2.8.2 (http://weblogo.berkeley.edu) (100) with default color code. Amino acids are numbered according to their positions in the hCMV (Towne) IE1 sequence. Numbers corresponding to amino acids forming the hCMV IE1 NBM are printed in bold type, and residues essential for nucleosome and chromosome interaction are underlined.

Figure 1

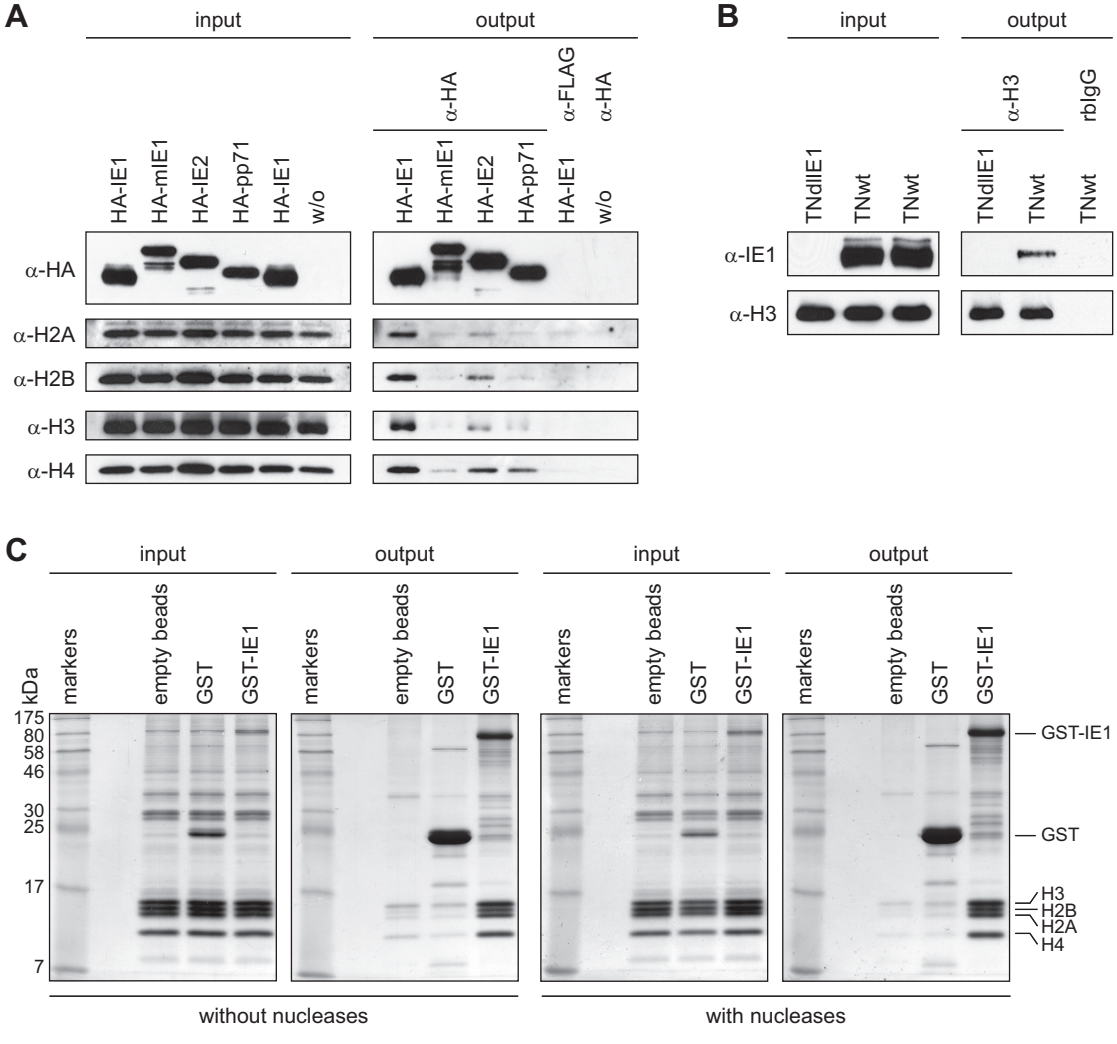
A
input
output
α-HA
α-FLAG
α-HA
HA-IE1
HA-mIE1
HA-IE2
HA-pp71
HA-IE1
w/o
HA-IE1
HA-mIE1
HA-IE2
HA-pp71
HA-IE1
w/o
α-HA
α-H2A
α-H2B
α-H3
α-H4
B
input
output
α-H3
rbIgG
TNdIIE1
TNwt
TNwt
TNdIIE1
TNwt
TNwt
α-IE1
α-H3
C
input
output
input
output
kDa
markers
empty beads
GST
GST-IE1
175
80
58
46
30
25
17
7
GST-IE1
GST
H3
H2B
H2A
H4
without nucleases
with nucleases

Figure 2

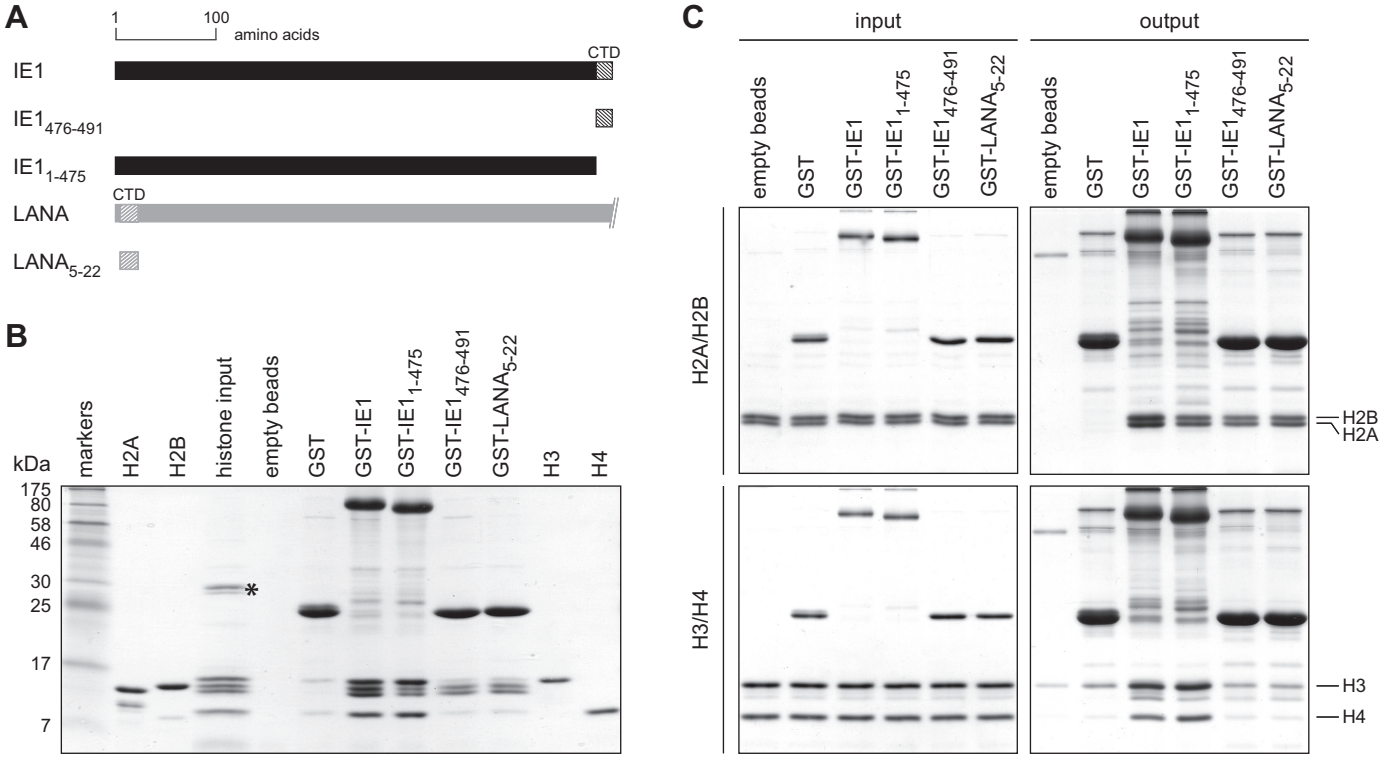
A
1
100
amino acids
IE1
CTD
IE1476-491
IE11-475
CTD
LANA
LANA5-22
B
kDa
markers
H2A
H2B
histone input
empty beads
GST
GST-IE1
GST-IE11-475
GST-IE1476-491
GST-LANA5-22
H3
H4
175
80
58
46
30
25
17
7
*
C
input
output
empty beads
GST
GST-IE1
GST-IE11-475
GST-IE1476-491
GST-LANA5-22
H2A/H2B
H3/H4
H2B
H2A
H3
H4

Figure 3

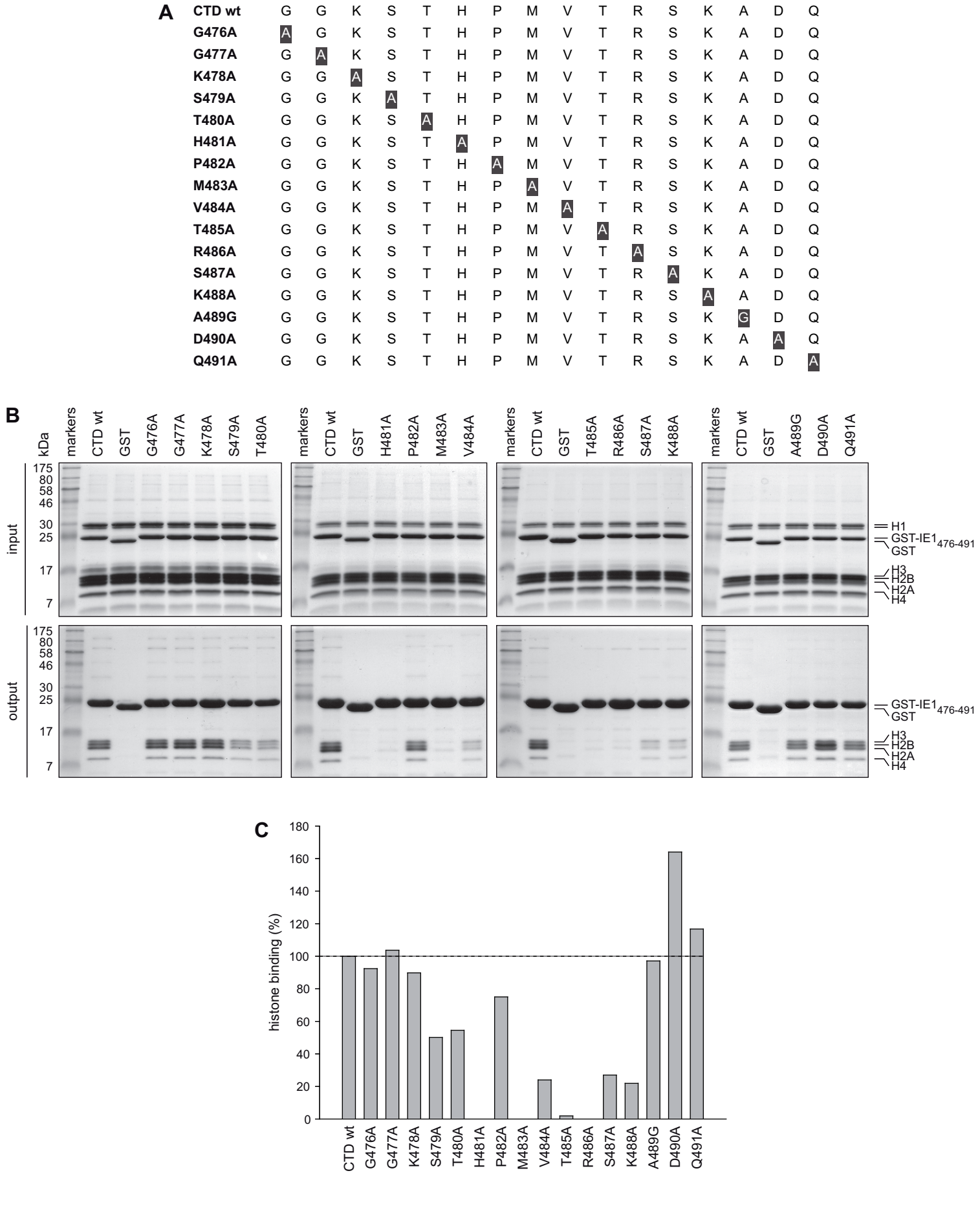
A
CTD wt G G K S T H P M V T R S K A D Q
G476A A G K S T H P M V T R S K A D Q
G477A G A K S T H P M V T R S K A D Q
K478A G G A S T H P M V T R S K A D Q
S479A G G K A T H P M V T R S K A D Q
T480A G G K S A H P M V T R S K A D Q
H481A G G K S T A P M V T R S K A D Q
P482A G G K S T H A M V T R S K A D Q
M483A G G K S T H P A V T R S K A D Q
V484A G G K S T H P M A T R S K A D Q
T485A G G K S T H P M V A R S K A D Q
R486A G G K S T H P M V T A S K A D Q
S487A G G K S T H P M V T R A K A D Q
K488A G G K S T H P M V T R S A A D Q
A489G G G K S T H P M V T R S K G D Q
D490A G G K S T H P M V T R S K A A Q
Q491A G G K S T H P M V T R S K A D A
B
kDa
markers
CTD wt
GST
G476A
G477A
K478A
S479A
T480A
H481A
P482A
M483A
V484A
T485A
R486A
S487A
K488A
A489G
D490A
Q491A
input
output
175
80
58
46
30
25
17
7
H1
GST-IE1476-491
GST
H3
H2B
H2A
H4
C
histone binding (%)
180
160
140
120
100
80
60
40
20
0

Figure 4

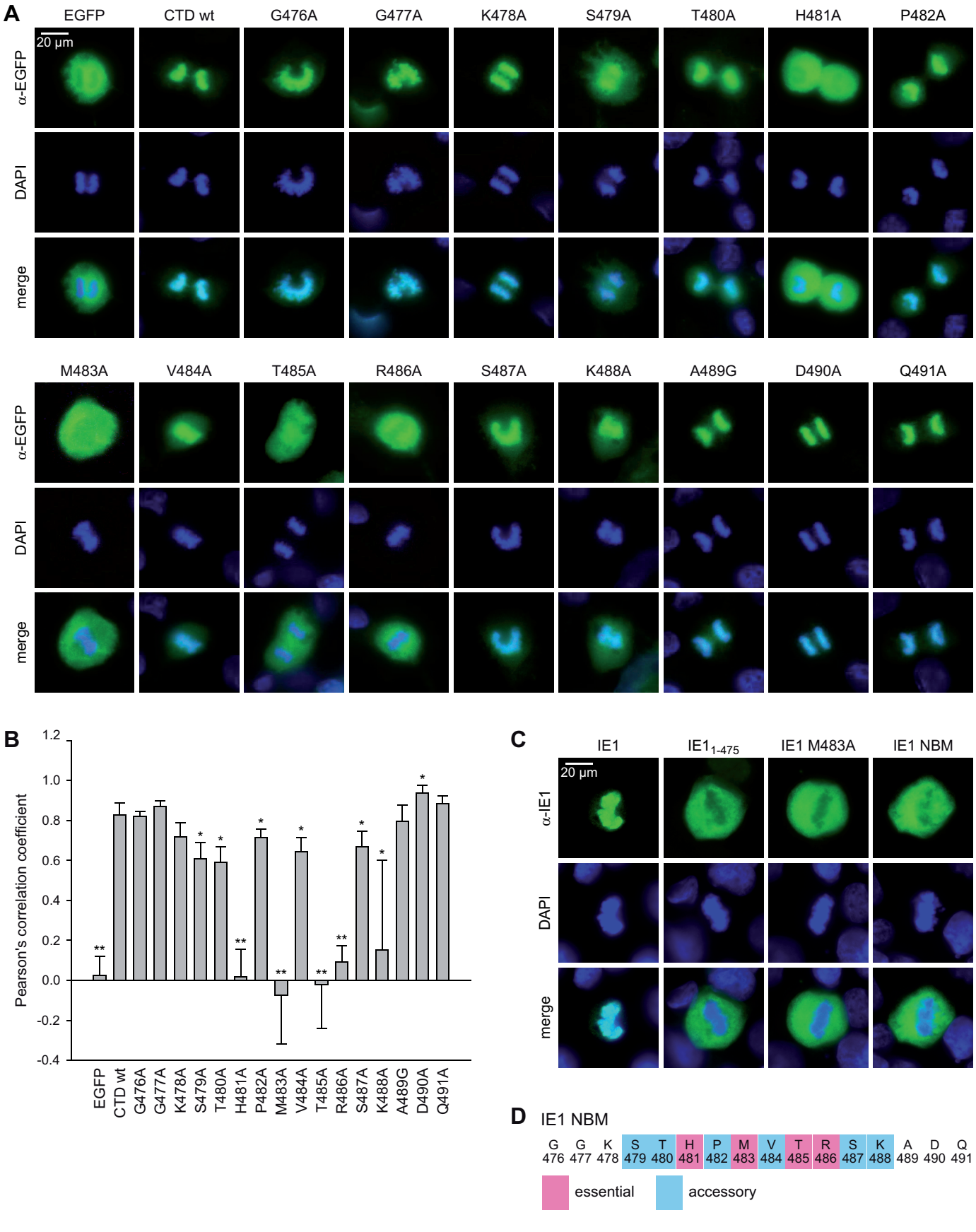
A
EGFP
CTD wt
G476A
G477A
K478A
S479A
T480A
H481A
P482A
20 µm
α-EGFP
DAPI
merge
M483A
V484A
T485A
R486A
S487A
K488A
A489G
D490A
Q491A
B
Pearson's correlation coefficient
1.2
1.0
0.8
0.6
0.4
0.2
0.0
-0.2
-0.4
EGFP
CTD wt
G476A
G477A
K478A
S479A
T480A
H481A
P482A
M483A
V484A
T485A
R486A
S487A
K488A
A489G
D490A
Q491A
C
IE1
IE1 1-475
IE1 M483A
IE1 NBM
20 µm
α-IE1
DAPI
merge
D
IE1 NBM
G 476
G 477
K 478
S 479
T 480
H 481
P 482
M 483
V 484
T 485
R 486
S 487
K 488
A 489
D 490
Q 491
essential
accessory

Figure 5

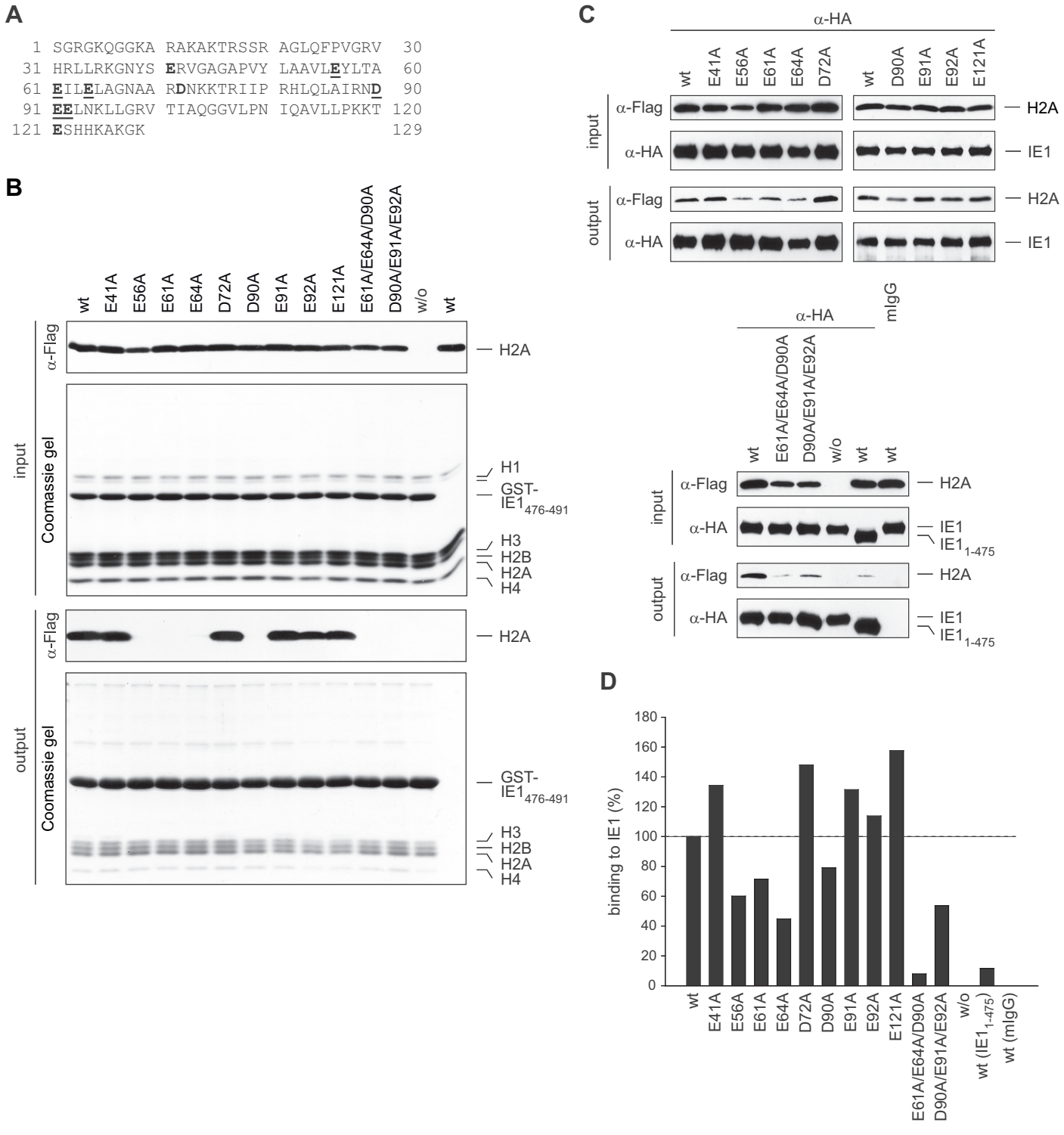
A
1 SGRGKQGGKA RAKAKTRSSR AGLQFPVGRV 30
31 HRLLRKGNYS ERVGAGAPVY LAAVLEYLTA 60
61 EILELAGNAA RDNKKTRIIP RHLQLAIRND 90
91 EELNKLLGRV TIAQGGVLPN IQAVLLPKKT 120
121 ESHHKAKGK 129
B
wt
E41A
E56A
E61A
E64A
D72A
D90A
E91A
E92A
E121A
E61A/E64A/D90A
D90A/E91A/E92A
w/o
wt
α-Flag
input
Coomassie gel
output
H2A
H1
GST-IE1476-491
H3
H2B
H2A
H4
C
α-HA
α-Flag
α-HA
input
output
H2A
IE1
mIgG
IE1
IE11-475
D
binding to IE1 (%)
180
160
140
120
100
80
60
40
20
0
wt (IE11-475)
wt (mIgG)

Figure 6

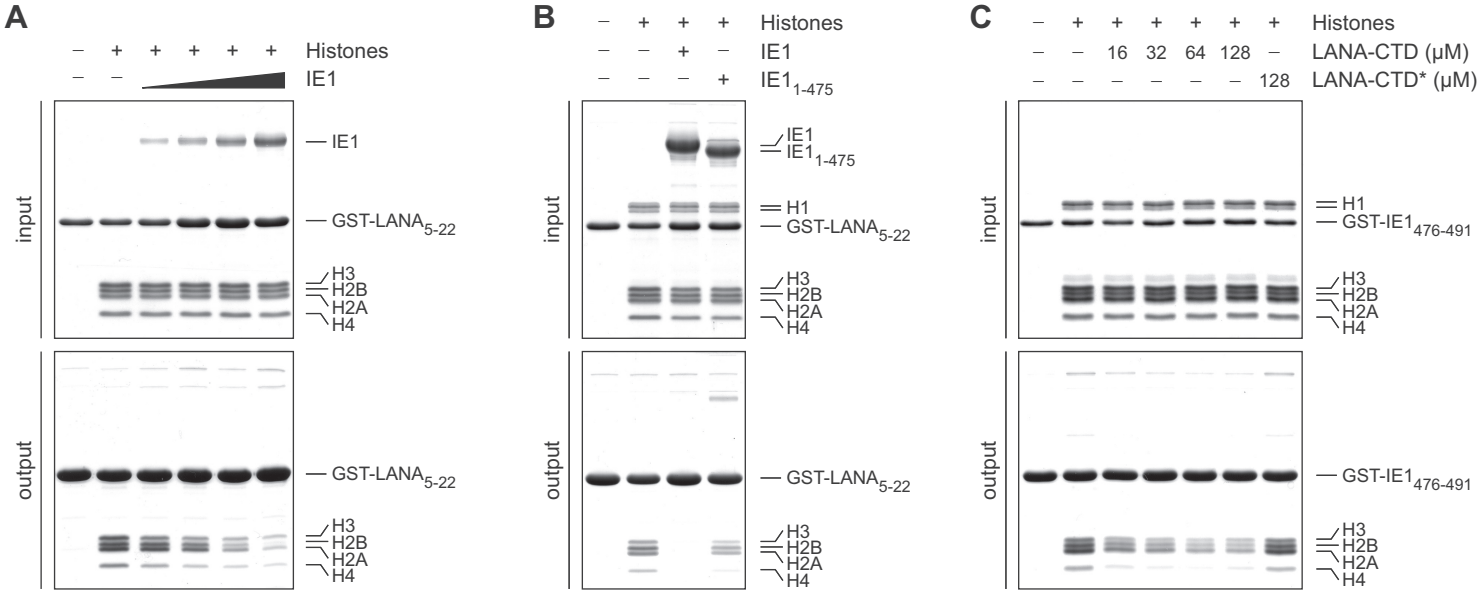
A
– + + + + + Histones
– – IE1
input
output
IE1
GST-LANA5-22
H3
H2B
H2A
H4
B
– + + + Histones
– – + – IE1
– – – + IE11-475
IE1
IE11-475
H1
C
– + + + + + + Histones
– – 16 32 64 128 – LANA-CTD (μM)
– – – – – – 128 LANA-CTD* (μM)
GST-IE1476-491

Figure 7

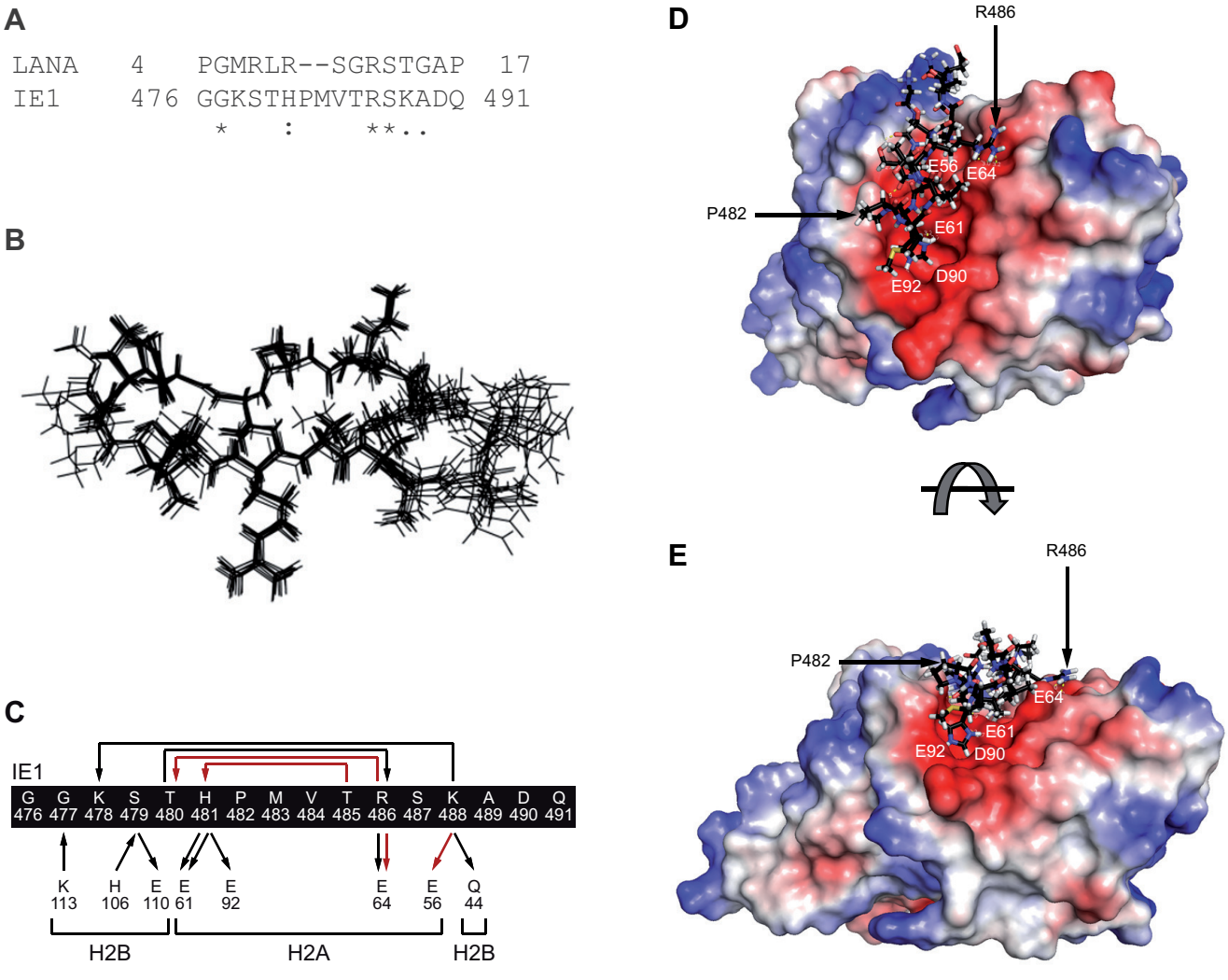
A
LANA 4 PGMRLR--SGRSTGAP 17
IE1 476 GGKSTHPMVTRSKADQ 491
* : **..
B
C
IE1
G G K S T H P M V T R S K A D Q
476 477 478 479 480 481 482 483 484 485 486 487 488 489 490 491
K 113
H 106
E 110
E 61
E 92
E 64
E 56
Q 44
H2B
H2A
H2B
D
R486
E56
E64
P482
E61
E92
D90
E
R486
P482
E64
E61
E92
D90

Figure 8

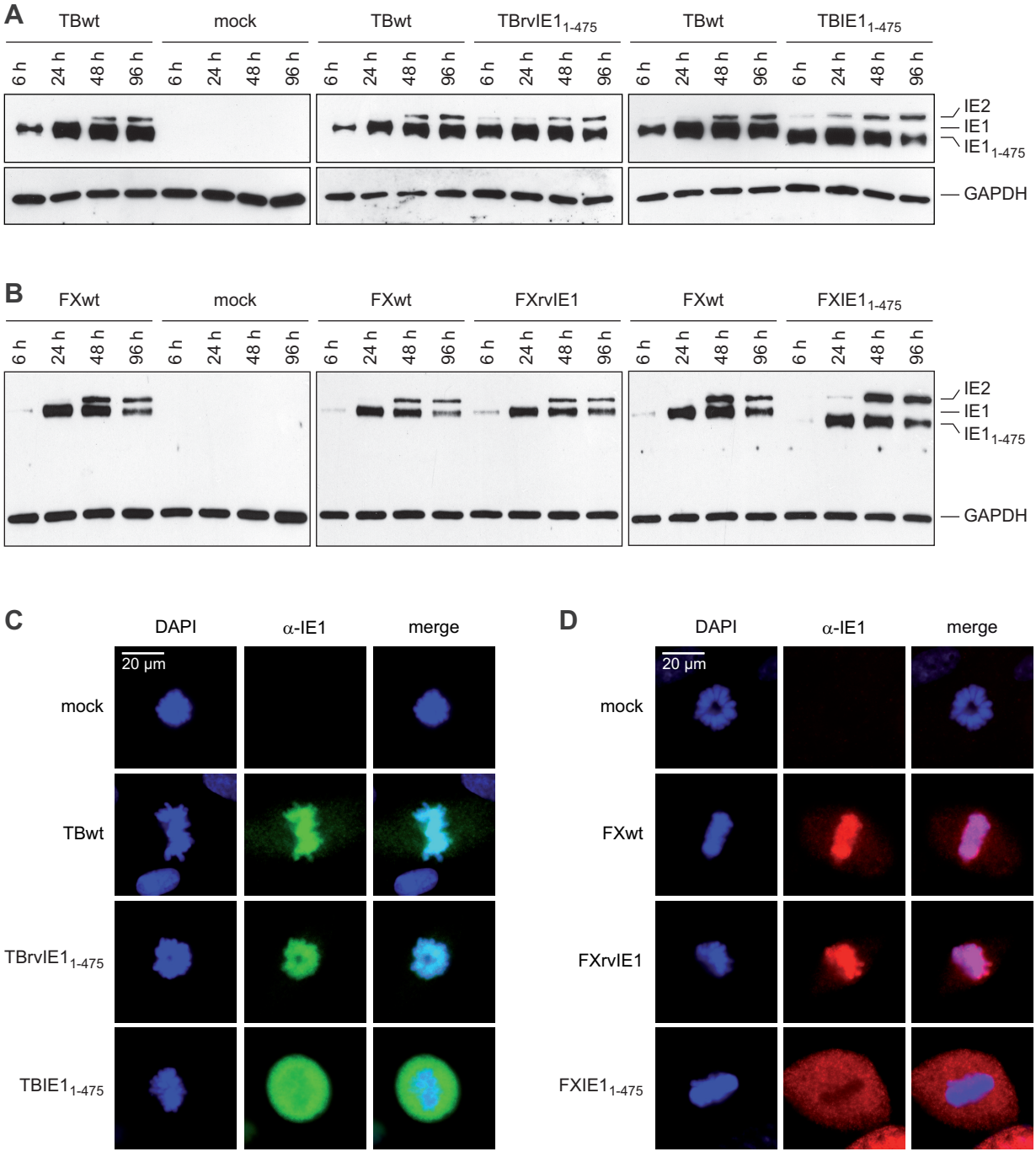
A
TBwt
mock
TBwt
TBrvIE1 1-475
TBwt
TBIE1 1-475
6 h
24 h
48 h
96 h
IE2
IE1
IE1 1-475
GAPDH
B
FXwt
mock
FXwt
FXrvIE1
FXwt
FXIE1 1-475
C
DAPI
α-IE1
merge
20 µm
mock
TBwt
TBrvIE1 1-475
TBIE1 1-475
D
FXwt
FXrvIE1
FXIE1 1-475

Figure 9

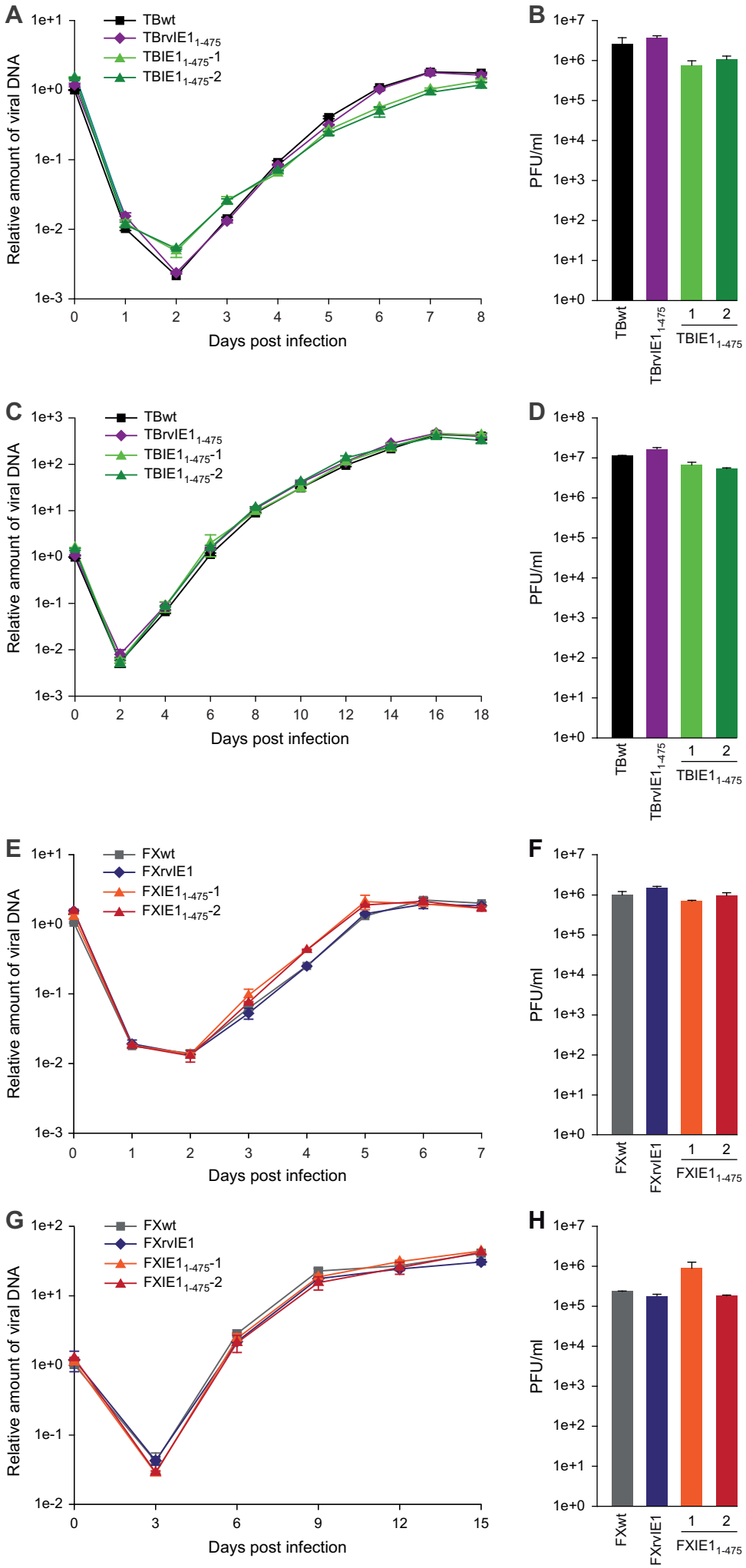
A
Relative amount of viral DNA
TBwt
TBrvIE1 1-475
TBIE1 1-475-1
TBIE1 1-475-2
Days post infection
B
PFU/ml
TBwt
TBrvIE1 1-475
1
2
TBIE1 1-475
C
Relative amount of viral DNA
TBwt
TBrvIE1 1-475
TBIE1 1-475-1
TBIE1 1-475-2
Days post infection
D
PFU/ml
TBwt
TBrvIE1 1-475
1
2
TBIE1 1-475
E
Relative amount of viral DNA
FXwt
FXrvIE1
FXIE1 1-475-1
FXIE1 1-475-2
Days post infection
F
PFU/ml
FXwt
FXrvIE1
1
2
FXIE1 1-475
G
Relative amount of viral DNA
FXwt
FXrvIE1
FXIE1 1-475-1
FXIE1 1-475-2
Days post infection
H
PFU/ml
FXwt
FXrvIE1
1
2
FXIE1 1-475

Figure 10

A

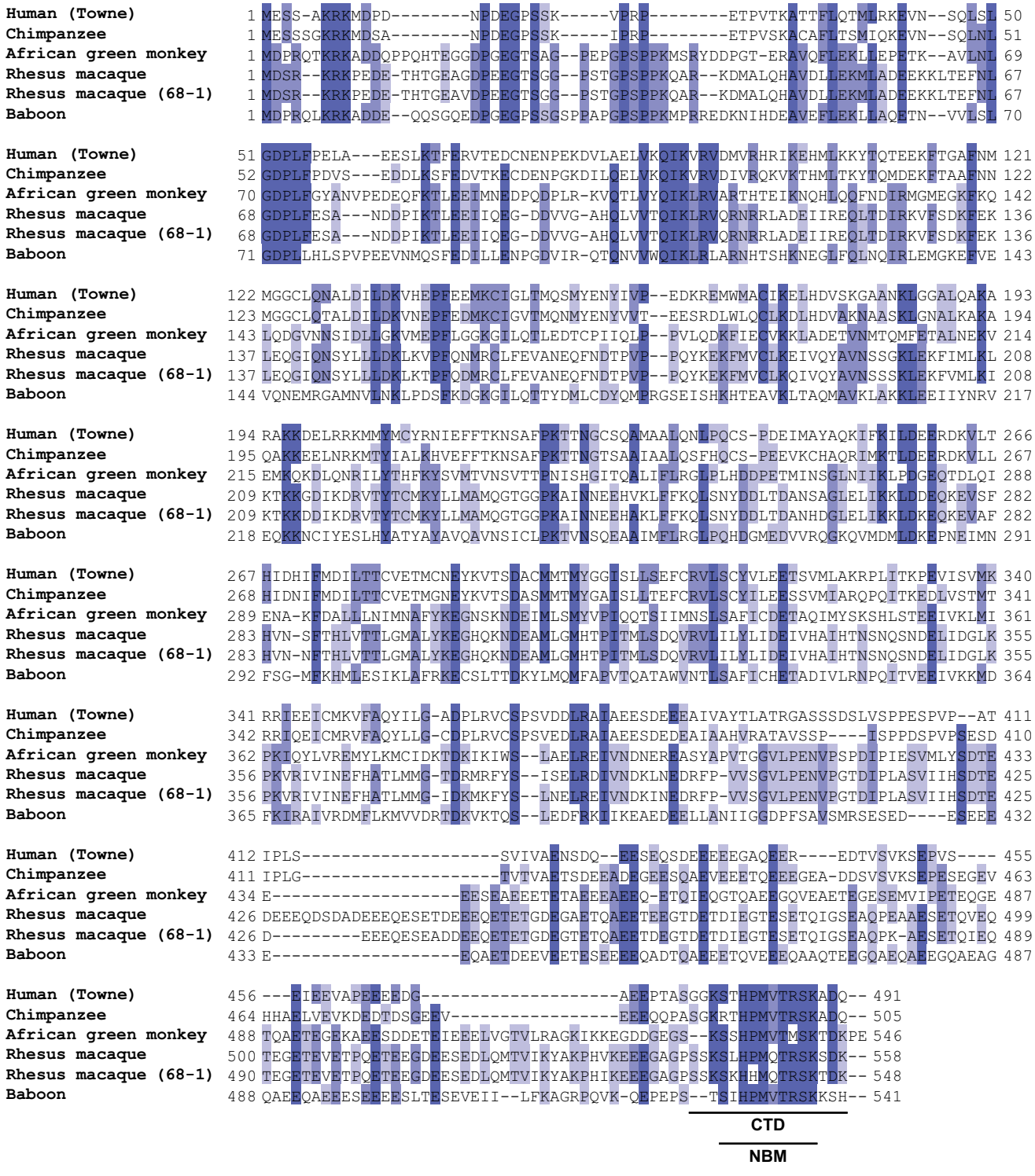

B

GenBank	CMV	IE1	CTD	NBM
AAR31448	Human (Towne)	100	100	100
AAM00752	Chimpanzee	67.2	87.5	90.0
AAB16882	African green monkey	26.3	62.5	80.0
AAB00487	Rhesus macaque	25.1	62.5	80.0
AAZ80666	Rhesus macaque (68-1)	24.2	56.3	70.0
ACX71624	Baboon	23.9	56.3	90.0

C